Slow relaxation of the magnetization, reversible solvent exchange and luminescence in 2D anilato-based frameworks

Samia Benmansour,*[a] Antonio Hernández-Paredes,[a] Arpan Mondal,[b] Gustavo López Martínez,[a] Josep Canet-Ferrer,[a] Sanjit Konar[b] and Carlos J. Gómez-García*[a]

Supporting Information

SYNTHESIS

Synthesis of compounds 1-3

Bromanilic acid ($H_2C_6O_4Br_2$, Scheme S1), $Dy(NO_3)_3{\cdot}5H_2O$ and all the solvents are commercially available and were used as received without further purification. The reactions were performed in open air.

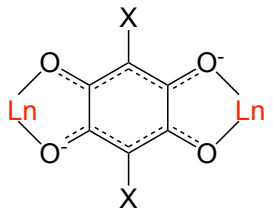

X = H, Cl, Br, Cl/CN,…

Scheme 1. Anilato-type ligands and their bis-bidentate coordination mode.

Synthesis of $[Dy_2(C_6O_4Br_2)_3(H_2O)_6]{\cdot}8H_2O$ (1)

This compound was obtained in a one-pot synthesis as a polycrystalline sample by adding, drop-wise, a solution of $Dy(NO_3)_3{\cdot}5H_2O$ (0.3 mmol, 131.6 mg) in 75 mL of H_2O to a solution of $H_2C_6O_4Br_2$ (0.45 mmol, 134.1 mg) in 150 mL of H_2O at 40 ºC. A purplish grey solid immediately appears. After stirring 30 min at 40 ºC the solution was cooled and the compound filtered and air dried. Yield: 81 %; elemental analysis calcd (%) for $C_{18}H_{28}O_{26}Br_6Dy_2$ (1464.83): C, 14.76; H, 1.93. Found: C, 15.21; H, 1.47. FT-IR (ν/cm^{-1}, KBr pellets): 3448 (m), 1612 (m), 1515 (vs), 1475 (s), 1379 (m), 1281 (w), 1094 (w), 990 (w), 814 (m), 565 (m) 452 (m).

Isostructural single crystals of the Yb(III) compound (compound **1-Yb**) were obtained by carefully layering in a thin tube at room temperature a solution of $H_2C_6O_4Br_2$ (4.5 mg, 0.015 mmol) in 2.5 mL of methanol onto a solution of $Yb(NO_3)_3 \cdot 5H_2O$ (4.5 mg, 0.010 mmol) in 2.5 mL of water. The tube was sealed and allowed to stand undisturbed. After eight days, purple hexagonal prismatic single crystals were formed in the interface.[1]

Synthesis of $[Dy_2(C_6O_4Br_2)_3(dmf)_6]$ (2)

This compound was obtained as compound **1** but using 15 mL of dmf for the $Dy(NO_3)_3 \cdot 5H_2O$ solution and 15 mL of dmf for the $H_2C_6O_4Br_2$ solution instead of H_2O. A violet polycrystalline solid is obtained. Yield: 69 %; elemental analysis calcd (%) for $C_{36}H_{42}N_6O_{18}Br_6Dy_2$ (1651.17): C, 26.19; H, 2.56; N, 5.10. Found: C, 21.30; H, 1.68; N, 3.02. FT-IR (ν/cm^{-1}, KBr pellets): 3423 (m), 2928 (w), 1647 (s), 1516 (vs), 1383 (s), 1281 (w), 1109 (w), 987 (w), 812 (m), 681 (w), 565 (m), 454 (m).

The low found N and H values indicate that this compound loses dmf molecules when stored in open air. In fact, to solve the structure, the single crystal was freshly picked from its mother liquor and immediately coated with paratone oil in order to avoid solvent loss. This solvent loss is further confirmed by the X-ray powder diffraction and TGA analysis (see below).

Red prism-shaped single crystals of **2** were obtained by carefully layering, at room temperature, a solution of $H_2C_6O_4Br_2$ (0.02 mmol, 5.96 mg) in 5 mL of methanol onto a solution of $Dy(NO_3)_3 \cdot 5H_2O$ (0.02 mmol, 8.77 mg) in 5 mL of dmf. The tube was sealed and allowed to stand for about two months. Suitable crystals for X-ray diffraction were freshly picked and covered with paratone oil in order to avoid solvent loss to be characterized by single crystal X-ray diffraction.

Synthesis of $[Dy_2(C_6O_4Br_2)_3(dmso)_4] \cdot 2dmso \cdot 2H_2O$ (3)

This compound was obtained as compound **1** but using 30 mL of dmso for the $Dy(NO_3)_3 \cdot 5H_2O$ solution and 30 mL of dmso for the $H_2C_6O_4Br_2$ solution instead of H_2O. In this compound, after 30 min of stirring at 40 ºC the solution was covered and allowed to stand at room temperature. Two days later, a dark purple solid precipitated. The solution was filtered and air dried. Yield: 63 % elemental analysis calcd (%) for

$C_{30}H_{40}O_{20}S_6Br_6Dy_2$ (1717.47): C, 20.98; H, 2.35; S, 11.20. Found: C, 20.81; H, 2.02; S, 10.29. FT-IR (ν/cm^{-1}, KBr pellets): 3422 (m), 2998 (w), 2919 (w), 1572 (m), 1498 (vs), 1411 (m), 1373 (s), 1283 (w), 1023 (m), 999 (m), 961 (m), 812 (m), 713 (w), 567 (m), 455 (m).

Single crystals of **3** were obtained, by the layering method as reported in our previous work.[2]

SOLVENT EXCHANGE

Solvent exchange for compound **1** was performed by immersing a polycrystalline sample of **1** in dmf to obtain **1/dmf**. The solvent was replaced every 24 hours during five days. After five days the compound was filtered and air dried. The same procedure was performed to exchange the solvents in compounds **2** (with dmso) and **3** (with H_2O), as summarized in **Table·S1** and **Scheme S2**.

The samples were also checked for reversibility. Thus, compound **1/dmf** was immersed into H_2O to obtain **1/dmf/H_2O** that contains H_2O and, therefore, is equivalent to the original compound **1**. This procedure was repeated for all the exchanged samples in order to check for reversibility in all cases.

These solvent exchanges show that it is possible to obtain any of the three compounds starting from any of the other two. The reversibility of the solvent exchange was confirmed with IR spectroscopy, TGA, Elemental analysis and XRPD (see below).

Table S1. Compounds and yields obtained by solvent exchange.

Compound	Formula	Solvent exchanged	Yield (%)
1	$[Dy_2(C_6O_4Br_2)_3(H_2O)_6]\cdot 8H_2O$		
1/dmf	$[Dy_2(C_6O_4Br_2)_3(dmf)_6]$	H_2O by dmf	97
3/H_2O/dmso	$[Dy_2(C_6O_4Br_2)_3(dmso)_4]\cdot 2dmso\cdot 2H_2O$	H_2O by dmso	80
2	$[Dy_2(C_6O_4Br_2)_3(dmf)_6]$		
2/dmso	$[Dy_2(C_6O_4Br_2)_3(dmso)_4]\cdot 2dmso\cdot 2H_2O$	dmf by dmso	53
1/dmf/H_2O	$[Dy_2(C_6O_4Br_2)_3(H_2O)_6]\cdot 8H_2O$	dmf by H_2O	85
3	$[Dy_2(C_6O_4Br_2)_3(dmso)_4]\cdot 2dmso\cdot 2H_2O$		
2/dmso/dmf	$[Dy_2(C_6O_4Br_2)_3(dmf)_6]$	dmso by dmf	37
3/H_2O	$[Dy_2(C_6O_4Br_2)_3(H_2O)_6]\cdot 8H_2O$	dmso by H_2O	70

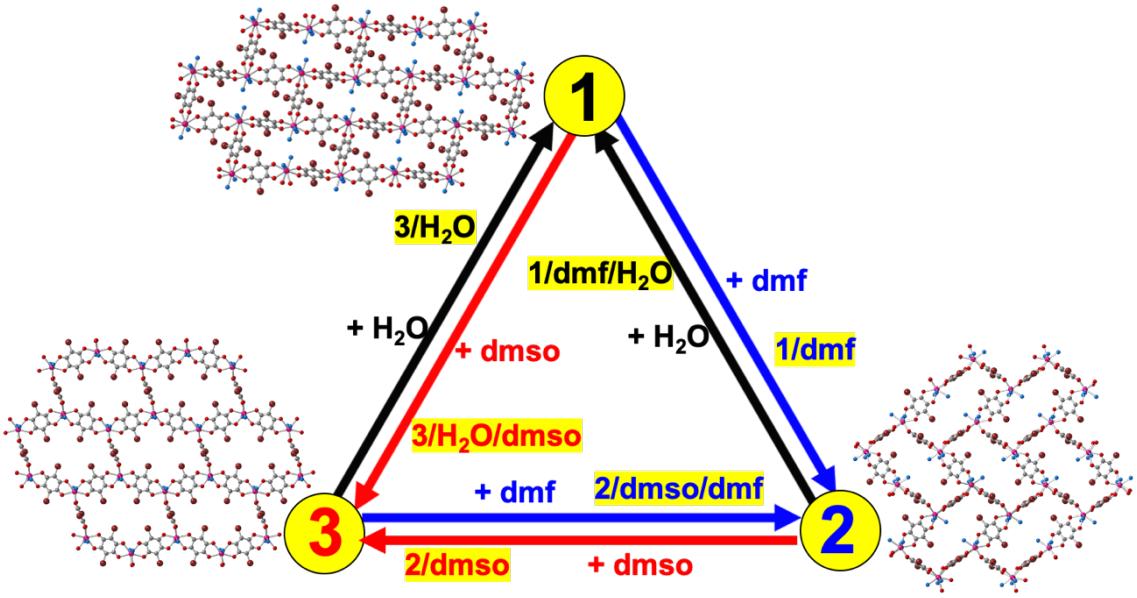

Scheme S2. Solvent exchange scheme for compounds **1**-**3**.

X-RAY SINGLE CRYSTAL STRUCTURE DETERMINATION

Suitable crystals of compounds **1**-**3** were selected and mounted on a mylar loop, coated with paratone oil and then transferred directly to the cold-nitrogen stream for data collection. X-ray data were collected at 120 K using ω scans on a Supernova diffractometer equipped with a graphite-monochromated Enhance (Mo) X-ray source (λ = 0.71073 Å). The program CrysAlisPro, Oxford Diffraction Ltd., was used for unit cell determinations, data reduction, scaling and for a multi-scan absorption correction using spherical harmonicsas implemented in SCALE3 ABSPACK.

The structures were solved in the space groups *P*-1 (for **1** and **3**) and $P2_1/n$ (for **2**) determined with the ShelXT structure solution program using the Intrinsic Phasing solution method and by using Olex2[3] as the graphical interface. The model was refined with version 2017/1 of XL[4] using Least Squares minimization. All non-hydrogen atoms were refined anisotropically. Hydrogen atom positions were calculated geometrically and refined using the riding model. Data collection and refinement parameters are provided in Table S2. Figures S1-S7 show details of the structures of the three compounds. CCDC files 1565283, 2005220 and 1579873 contain the supplementary crystallographic information of compounds **1**-**3**, respectively. Note that the structure of compound **3** was recently published by some of us.[2]

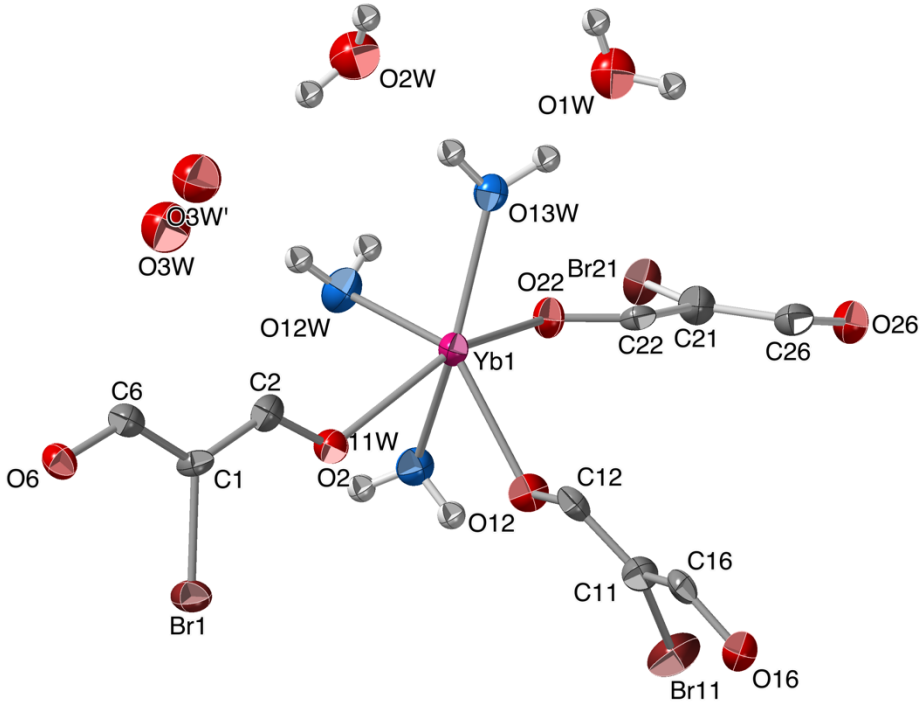

Figure S1. Asymmetric unit with labels in compound **1**. Ellipsoids are drawn at 80 % probability.

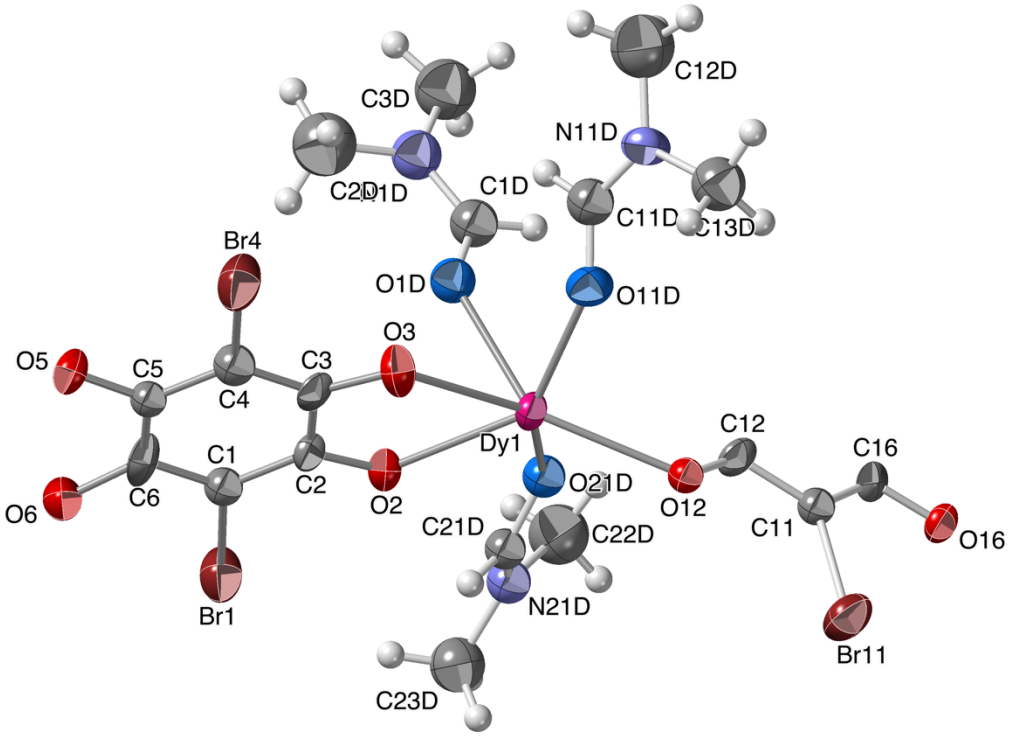

Figure S2. Asymmetric unit with labels in compound **2**. Ellipsoids are drawn at 80 % probability.

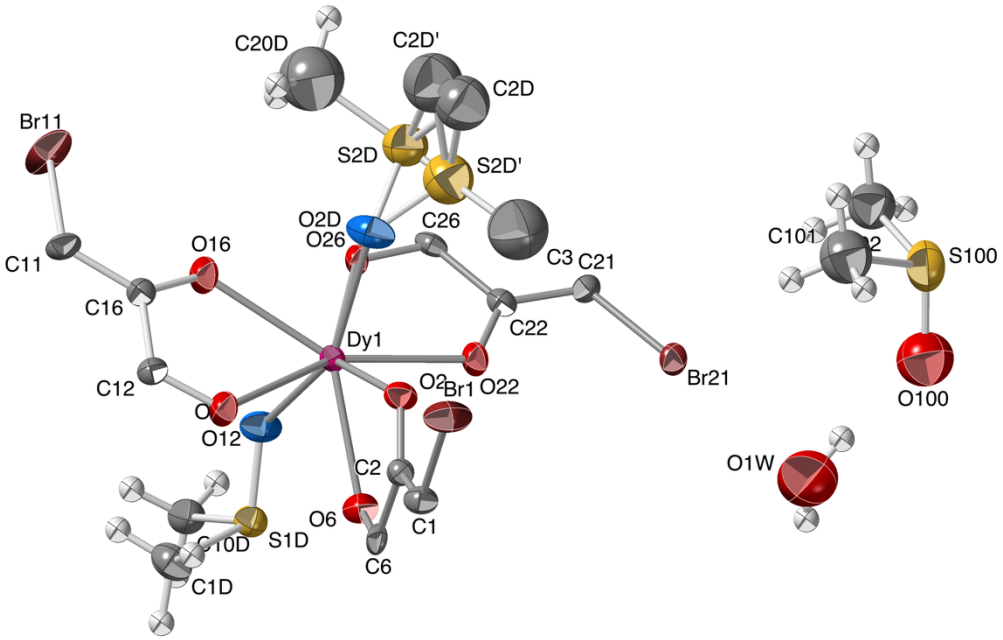

Figure S3. Asymmetric unit with labels in compound **3**. Ellipsoids are drawn at 80 % probability.

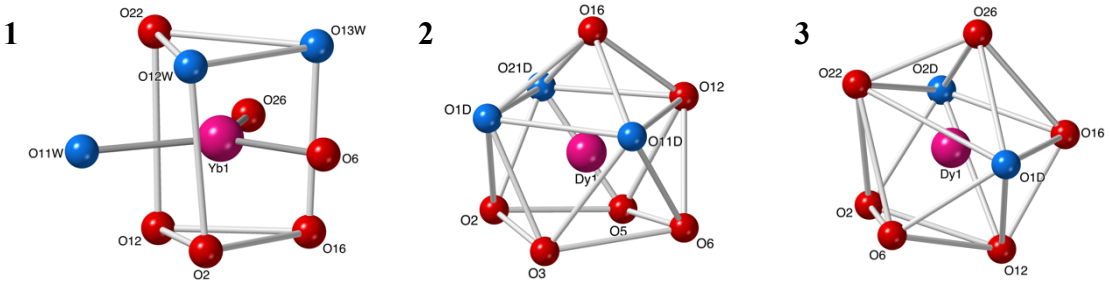

Figure S4. Coordination geometries in compounds **1**-**3**. Colour code: Ln(III) = pink, O(anilato) = red, O(solvent) = blue.

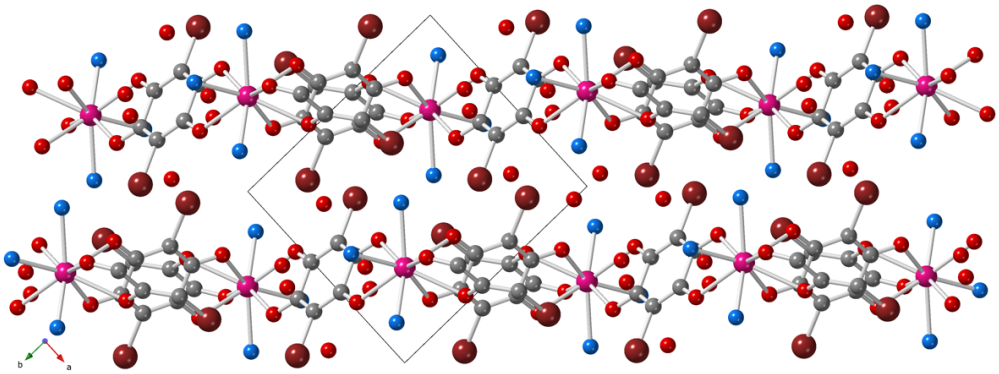

Figure S5. Side view of the layers in compound **1**. Colour code: Ln(III) = pink, O(anilato) = red, O(solvent) = blue. C = grey and Br = brown. Only the O atoms of the solvent molecules are displayed for clarity.

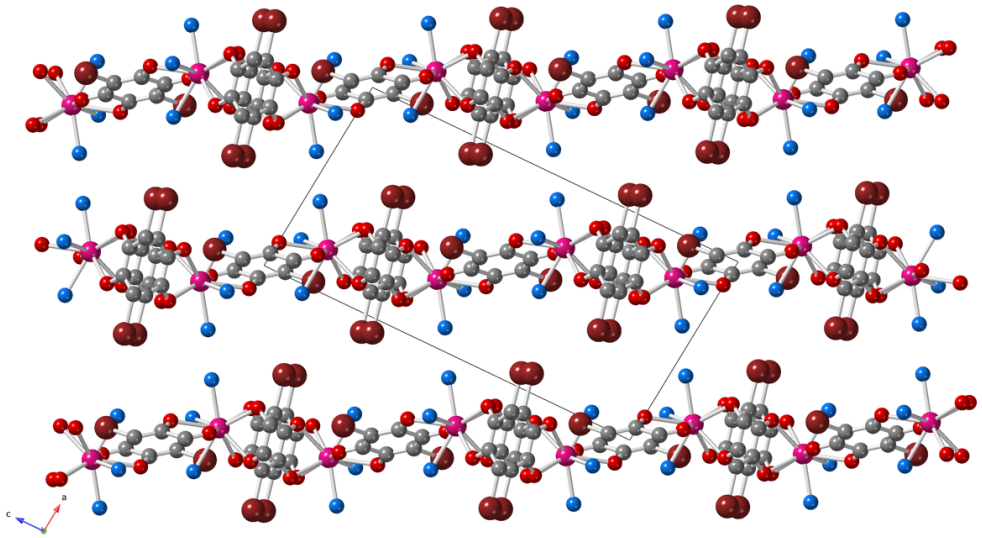

Figure S6. Side view of the layers in compound **2**. Colour code: Ln(III) = pink, O(anilato) = red, O(solvent) = blue. C = grey and Br = brown. Only the O atoms of the solvent molecules are displayed for clarity.

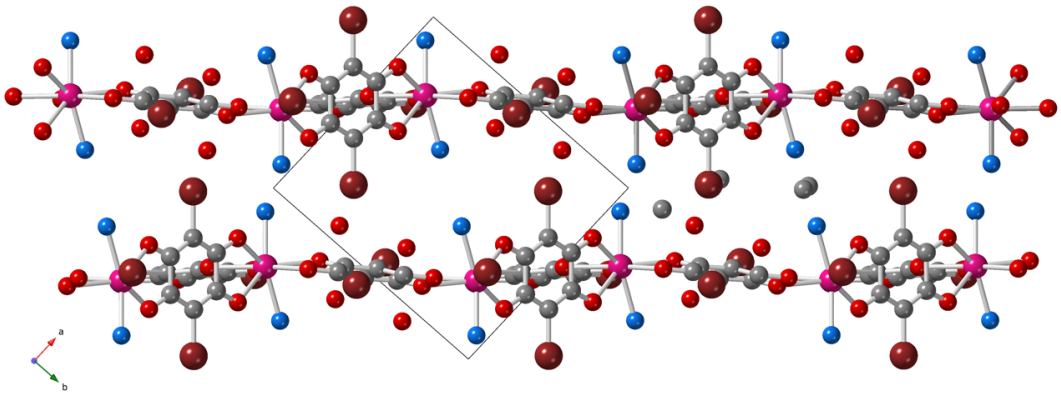

Figure S7. Side view of the layers in compound **3**. Colour code: Ln(III) = pink, O(anilato) = red, O(solvent) = blue. C = grey and Br = brown. Only the O atoms of the solvent molecules are displayed for clarity.

Table S2. Crystallographic data for compounds $[Dy_2(C_6O_4Br_2)_3(H_2O)_6]\cdot 8H_2O$ (**1**), $[Dy_2(C_6O_4Br_2)_3(dmf)_6]$ (**2**) and $[Dy_2(C_6O_4Br_2)_3(dmso)_4]\cdot 2dmso\cdot 2H_2O$ (**3**).

Compound	**1**	**2**	**3**
CCDC	1565283	2005220	1579873
Formula	$C_9H_{10}Br_3O_{12}Yb$	$C_{18}H_{21}Br_3DyN_3O_9$	$C_{15}H_{16.1}Br_3DyO_{10}S_3$
$D_{calc.}$ (g cm^{-3})	2.760	2.101	2.238
μ/mm^{-1}	12.322	7.505	7.963
Formula Weight	722.94	825.61	854.79
Colour	brown	violet	brown
Shape	block	block	prism
Size (mm^3)	0.13×0.08×0.06	0.13×0.07×0.04	0.08×0.04×0.03
T (K)	120.00(10)	119.7(9)	123.95(10)
Crystal System	triclinic	monoclinic	triclinic
Space Group	P-1	$P2_1/n$	P-1
a (Å)	9.0568(4)	10.0215(5)	9.9121(4)
b (Å)	10.2351(4)	13.4454(6)	10.6798(4)
c (Å)	10.9160(5)	19.4727(9)	12.7892(4)
α (°)	65.763(4)	90	78.919(3)
β (°)	70.612(4)	95.859(4)	72.796(3)
γ (°)	80.712(4)	90	85.035(3)
V (Å^3)	870.00(7)	2610.1(2)	1268.53(8)
Z	2	4	2
Wavelength (Å)	0.71073	0.71073	0.71073
Radiation type	MoKα	MoKα	MoKα
θ_{min} (°)	3.187	3.431	3.259
θ_{max} (°)	25.072	25.056	25.036
Measured Refl.	10897	17018	12273
Independent Refl.	3072	4602	4477
Reflections with I > 2σ(I)	2946	3575	4126
R_{int}	0.0334	0.0754	0.0273
Parameters	243	296	327
Restraints	27	111	64
Largest Peak	1.452	3.364	2.313
Deepest Hole	-0.979	-1.312	-1.161
GooF	1.043	1.123	1.049
R_1[a]	0.0224	0.0662	0.0270
R_1 (all data)	0.0237	0.0876	0.0303
wR_2[b]	0.0595	0.1603	0.0634
wR_2 (all data)	0.0608	0.1727	0.0651

[a] $R_1 = \sum||F_o|-|F_c||/\sum|F_o|$; [b] $wR_2\ (F_o^2) = [\sum[w(F_o^2 - F_c^2)^2/\sum w\ F_o^4]^{½}$.

CONTINUOUS SHAPE ANALYSIS

Table S3. Continuous SHAPE measurement (CShM)[5] values for the 13 possible coordination geometries found for coordination number nine[6] in compounds **1** and **2**. Minima values are indicated in bold.

Geometry	symmetry	1	2
EP-9	D_{9h}	35.948	37.207
OPY-9	C_{8v}	21.797	22.231
HBPY-9	D_{7h}	20.172	19.769
JTC-9	C_{3v}	14.665	16.104
JCCU-9	C_{4v}	10.347	9.813
CCU-9	C_{4v}	9.534	8.549
JCSAPR-9	C_{4v}	1.703	1.492
CSAPR-9	C_{4v}	0.732	**0.450**
JTCTPR-9	D_{3h}	1.688	2.422
TCTPR-9	D_{3h}	**0.595**	0.597
JTDIC-9	C_{3v}	12.052	11.588
HH-9	C_{2v}	11.954	12.432
MFF-9	C_s	1.469	0.995

EP-9 = Enneagon; OPY-9 = Octagonal pyramid; HBPY-9 = Heptagonal bipyramid; JTC-9 = Triangular cupola (J3) = trivacant cuboctahedron; JCCU-9 = Capped cube (Elongated square pyramid, J8); CCU-9 = Capped cube; JCSAPR-9 = Capped square antiprism (Gyroelongated square pyramid J10); **CSAPR-9 = Capped square antiprism**; JTCTPR-9 = Tricapped trigonal prism (J51); **TCTPR-9 = Tricapped trigonal prism**; JTDIC-9 = Tridiminished icosahedron (J63); HH-9 = Hula-hoop; MFF-9 = Muffin. The minima values are indicated in bold.

Table S4. Continuous SHAPE measurement (CShM)[5] values of the 13 possible coordination geometries for the Dy(III) ion with coordination number eight[7] in compound **3**. The minimum value is indicated in bold.

Geometry	Symmetry	3
OP-8	D_{8h}	30.485
HPY-8	C_{7v}	23.320
HBPY-8	D_{6h}	15.044
CU-8	O_h	11.632
SAPR-8	D_{4d}	1.823
TDD-8	$\mathbf{D_{2d}}$	**1.079**
JGBF-8	D_{2d}	12.734
JETBPY-8	D_{3h}	28.683
JBTP-8	C_{2v}	2.445
BTPR-8	C_{2v}	2.066
JSD-8	D_{2d}	2.836
TT-8	T_d	12.359
ETBPY-8	D_{3h}	23.895

OP-8 = Octagon; HPY-8 = Heptagonal pyramid; HBPY-8 = Hexagonal bipyramid; CU-8 = Cube; SAPR-8 = Square antiprism; **TDD-8 = Triangular dodecahedron**; JGBF-8 = Johnson-Gyrobifastigium (J26); JETBPY-8 = Johnson-Elongated triangular bipyramid (J14); JBTP-8 = Johnson-Biaugmentedtrigonal prism (J50); BTPR-8 = Biaugmentedtrigonal prism; JSD-8 = Snub disphenoid (J84); TT-8 = Triakis tetrahedron.

X-RAY POWDER DIFFRACTION (XRPD)

The X-ray powder diffractograms were collected for polycrystalline samples filled into 0.7 mm glass capillaries that were mounted and aligned on a Empyrean PANalytical powder diffractometer, using CuKα radiation (λ = 1.54177 Å). A total of 3 scans were collected at room temperature in the range 5-40º.

Experimental X-ray powder diffractogram of a polycrystalline sample of compound **1** prepared by the one-pot method shows that it is not isostructural with the corresponding single crystal obtained by the layering method (**1'**, that contains 12 crystallization water molecules and we call phase I).[1] Fortunately, compound **1** is isostructural with the single crystals obtained with the two smaller lanthanoids: Tm(III) and Yb(III) (compounds **1-Tm** and **1-Yb**, that contain only eight crystallization water molecules and we call phase II). Accordingly, we will compare the XRPD of compound **1** with the generated from the single crystal structure of **1-Yb**. This fact indicates that the phase with eight water molecules (phase II) is the kinetic phase since it is obtained for short crystallization times (one-pot method) whereas the phase with twelve water molecules (phase I) is the thermodynamic one since it is obtained for long crystallization times (layering method). This finding is not only restricted to the Dy(III) derivative but is also found in all the Ln(III) from Sm(III) to Er(III) that crystallize in phase I (with 12 H_2O molecules) with the slow layering method but in phase II (with 8 H_2O molecules) with the fast precipitation one-pot method.[1]

In contrast, the experimental XRPD of **2** and **3** are similar to the simulated ones from the corresponding single crystal X-ray structures, indicating that **2** and **3** are isostructural with the corresponding single crystals obtained by layering method. Note that the samples with dmf lose solvent molecules (and crystallinity) very easily as also confirmed by the elemental analysis and thermogravimetric measurements (see below).

The X-ray powder diffractograms of the exchanged samples show that (i) the compounds with water as solvent (**1**, **1/dmf/H_2O** and **3/H_2O**) are isostructural (Figure S8); (ii) the three compounds with dmf as solvent (**2**, **1/dmf** and **2/dmso/dmf**) are isostructural (Figure S9) and (iii) the three compounds with dmso as solvent (**3**, **3/H_2O/dmso** and **2/dmso**) are also isostructural (Figure S10), confirming the solvent exchange in all cases and their reversibility.

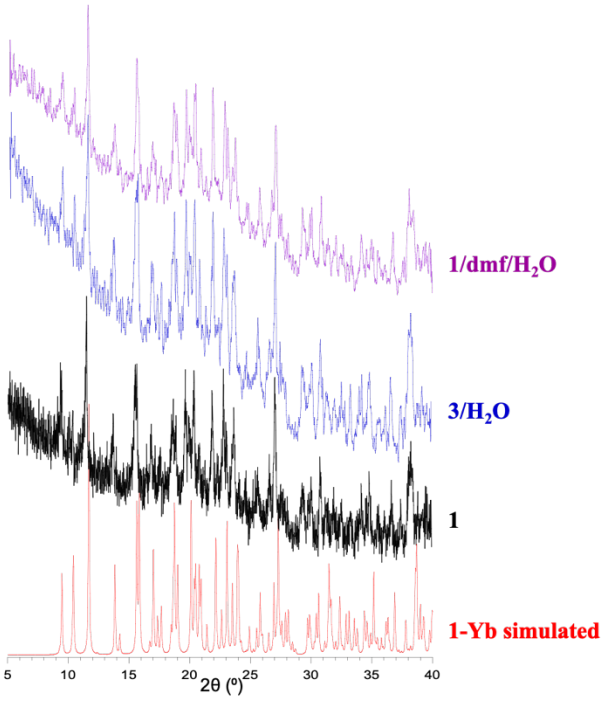

Figure S8. X-ray powder diffractograms of three compounds containing water as solvent (**1**, **3/H₂O** and **1/dmf/H₂O**) and the simulated one from the single crystal structure of compound **1-Yb**.

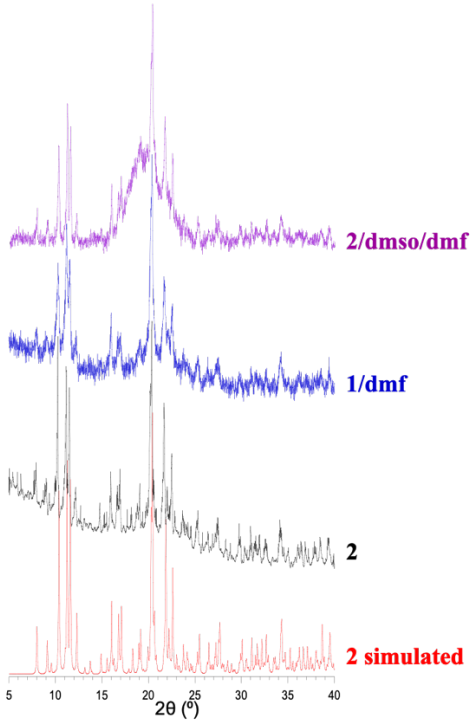

Figure S9. X-ray powder diffractogram of the three compounds containing dmf as solvent (**2**, **1/dmf** and **2/dmso/dmf**) and the simulated one from the single crystal structure of compound **2**.

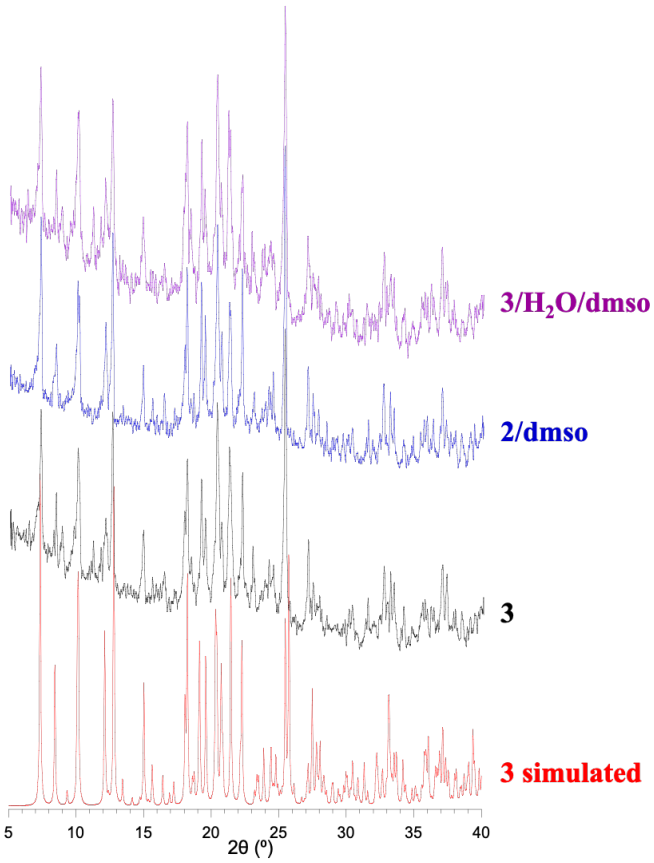

Figure S10. X-ray powder diffractograms of the three compounds containing dmso as solvent (**3**, **2/dmso** and **3/H$_2$O/dmso**) and the simulated one from the single crystal structure of compound **3**.

INFRARED SPECTROSCOPY (FT-IR)

FT-IR spectra were performed on KBr pellets and collected with a Bruker Equinox 55 spectrometer.

Compounds **1**-**3** show very similar IR spectra with differences attributed to the different coordinated solvent in each compound: water for **1**, dmf for **2** and dmso for **3** (Figures S11-S13). The IR spectra confirm that the solvent exchange and its reversibility have been successfully carried out.

The main bands and their assignments are shown in Tables S5-S7.

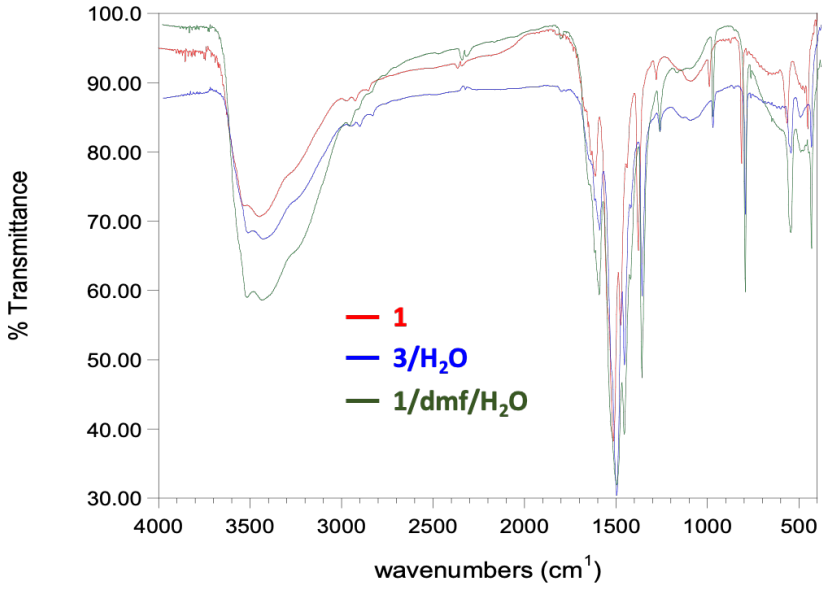

Figure S11. FT-IR spectra in the 4000-400 cm^{-1} region of of the three compounds containing H_2O as solvent (**1**, **1/dmf/H₂O** and **3/H₂O**).

Table S5. Selected vibrational frequencies (cm^{-1}) for compounds with water as solvent (**1, 1/dmf/H₂O** and **3/H₂O**).

band	1	1/dmf/H₂O	3/H₂O
Bending water	1612	1612	1612
ν(C=C) + ν(C-O)	1515	1518	1519
ν(C-C) + ν(C-O)	1379	1379	1379
δ(C-X)	814	814	814
ρ(C-X)	565	565	565

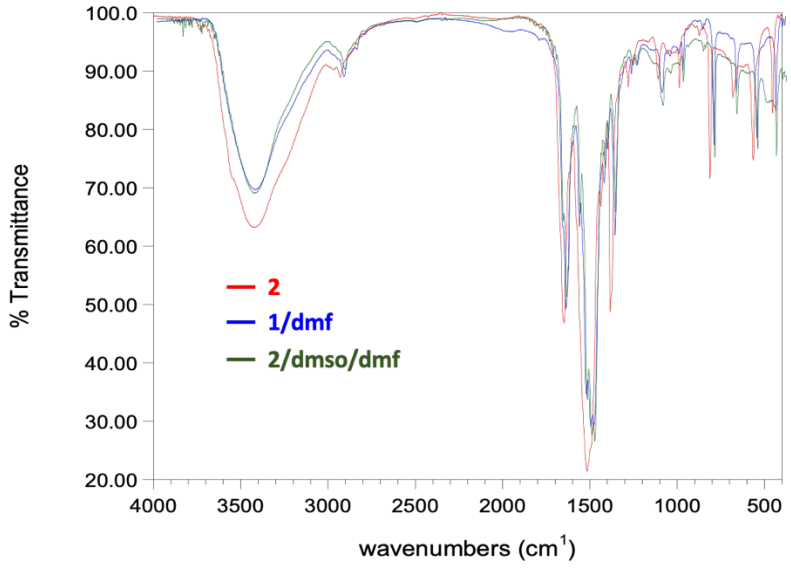

Figure S12. FT-IR spectra in the 4000-400 cm^{-1} region of of the three compounds containing dmf as solvent (**2**, **1/dmf** and **2/dmso/dmf**).

Table S6. Selected vibrational frequencies (cm^{-1}) for compounds with dmf as solvent (**2, 1/dmf** and **2/dmso/dmf**).

band	2	1/dmf	2/dmso/dmf
ν(C-H)$_{solvent}$	≈ 2927	2928	2927
ν(C=O)$_{solvent}$	1647	1657	1656
ν(C=C) + ν(C-O)	1516	1514	≈ 1515
ν(C-C) + ν(C-O)	1383	1375	1375
δ(C-X)	812	809	809
ρ(C-X)	565	564	563

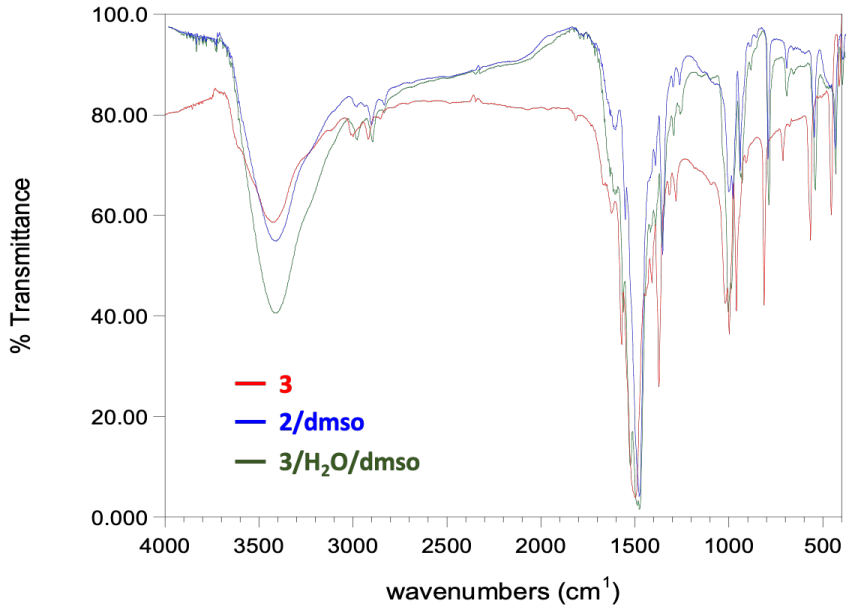

Figure S13. FT-IR spectra in the 4000-400 cm^{-1} region of of the three compounds containing dmso as solvent (**3**, **3/H_2O/dmso** and **2/dmso**).

Table S7. Selected vibrational frequencies (cm^{-1}) for compounds with dmso as solvent (**3, 3/H_2O/dmso** and **2/dmso**).

band	3	3/H_2O/dmso	2/dmso
ν(C-H)$_{solvent}$	2919	2999 2916	2921
ν(C=C) + ν(C-O)	1498	1495	1496
ν(C-C) + ν(C-O)	1373	1376	1373
ν(S=O)$_{solvent}$	≈ 1024	1023	≈ 1024
ρ(C-S)$_{solvent}$	961	951	960
δ(C-X)	812	808	812
ρ(C-X)	567	561	566

The reversibility of the solvent exchange can be further confirmed with IR spectroscopy as shown in Figures S14-S16.

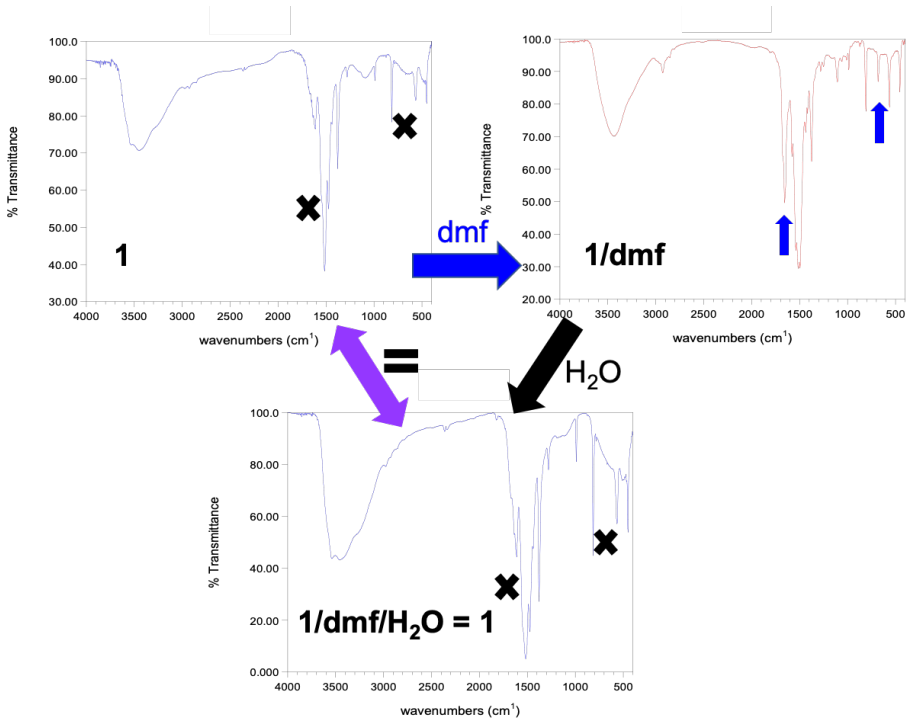

Figure S14. IR spectra showing the reversibility of compound **1** with dmf.

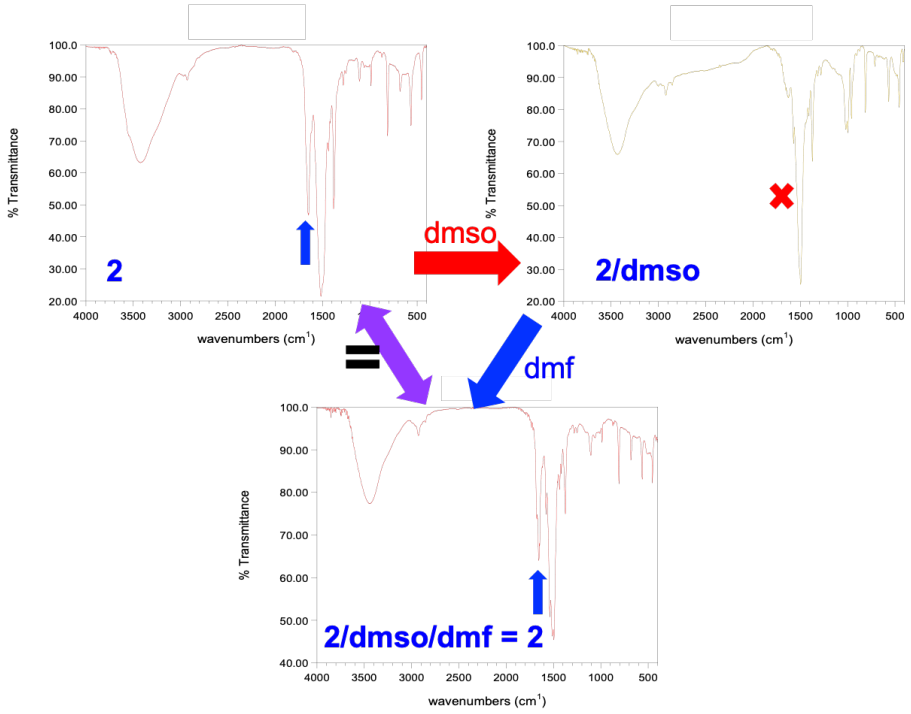

Figure S15. IR spectra showing the reversibility of compound **2** with dmso.

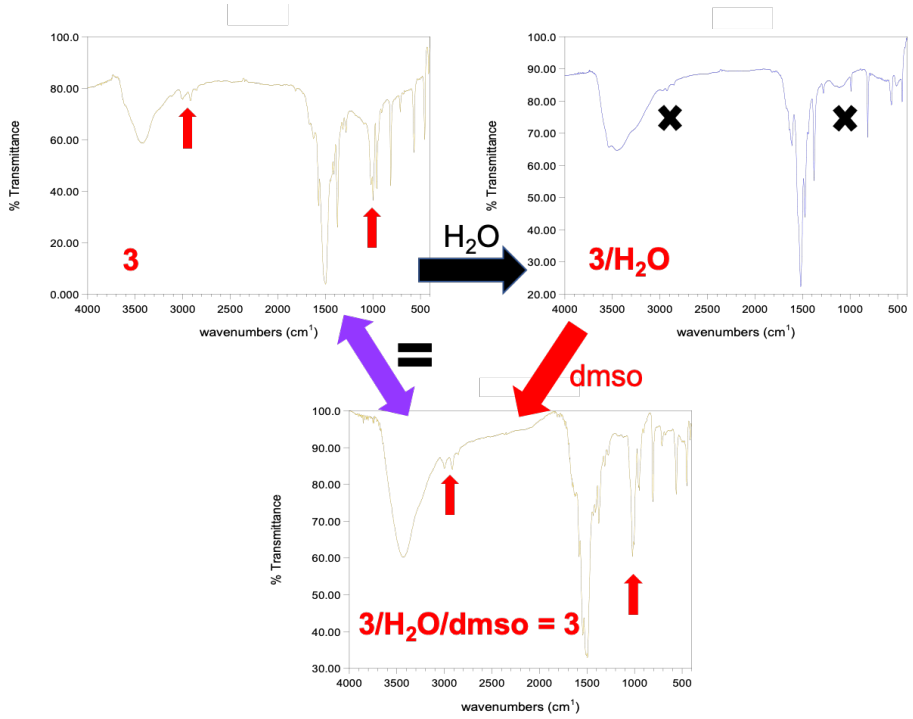

Figure S16. IR spectra showing the reversibility of compound **3** with H_2O.

THERMOGRAVIMETRIC ANALYSIS (TGA)

TGA measurements were performed in Pt crucibles with a TA instruments TGA 550 thermobalance equipped with an auto sampler. The measurements were done in the 25-400 ºC temperature range at 10ºC/min under N_2 flux of 60 mL/min.

Compound **1** shows an initial weight loss of *ca.* of 7 % in the temperature range 25-65 ºC corresponding to the release of *ca*. 6 crystallization water molecules. Additionally, in the 100-150 ºC range it shows a weight loss of *ca.* of 15 % consistent with the loss of the eight crystallization water molecules plus 4 coordinated water molecules (Figure S17). Compound **2** shows an initial smooth weight loss of *ca.* 4 % in the 25-50 ºC range (Figure S20), corresponding to the release of *ca*. 1 coordinated dmf molecules. Additionally, in the 150-300 ºC range it shows a smooth and progressive weight loss of *ca.* 13 % consistent with the loss of two more coordinated dmf molecules. Compound **3** shows an initial weight loss of *ca.* of 9 % in the range 25-100 ºC (Figure S23), indicating the release of two crystallization water molecules and one crystallization dmso molecule (see tables S8-S10).

In the exchanged samples, TGA measurements (Figures S17-S25) show that the solvent content in all cases agrees with the values found in the elemental analysis and

X-Ray crystal structure (Tables S8-S10). The only discrepancies correspond to the dmf-containing samples that show lower values due to the solvent loss when the samples are air dried at room temperatures.

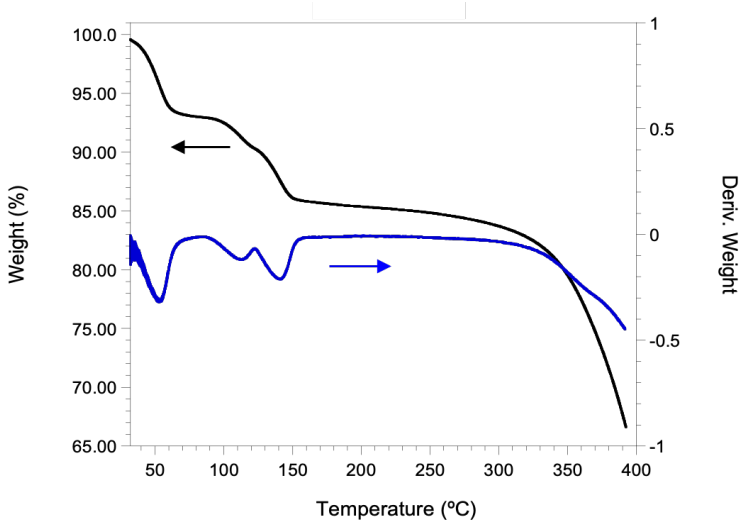

Figure S17. TG (left scale) and derivative (right scale) of compound **1**.

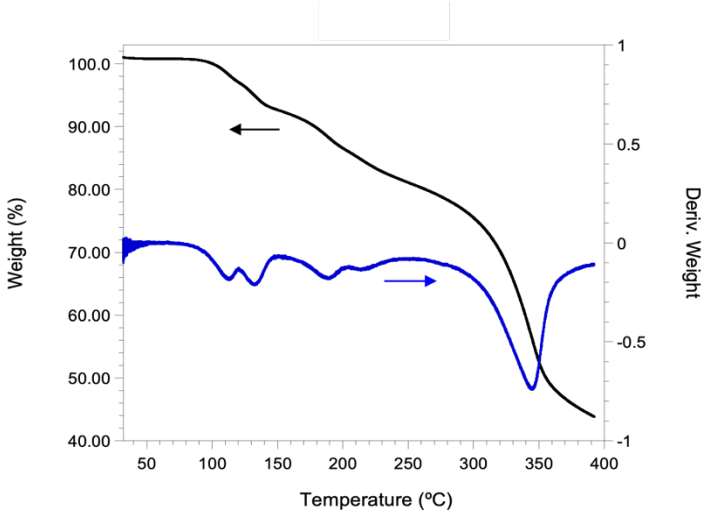

Figure S18. TG (left scale) and derivative (right scale) of compound **1/dmf**.

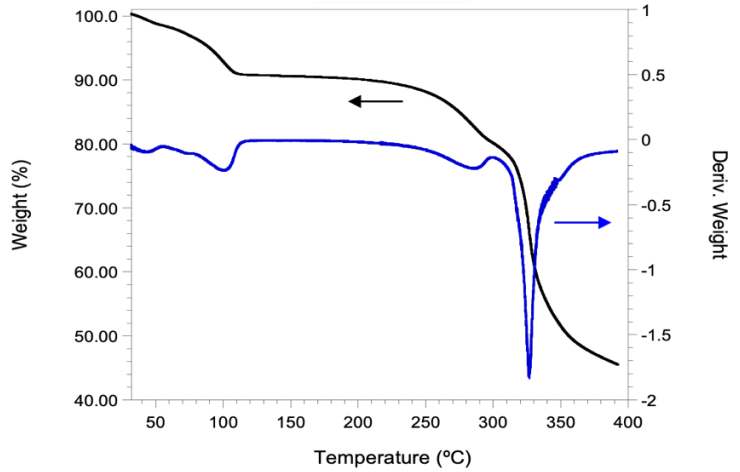

Figure S19. TG (left scale) and derivative (right scale) of compound **3/H_2O/dmso**.

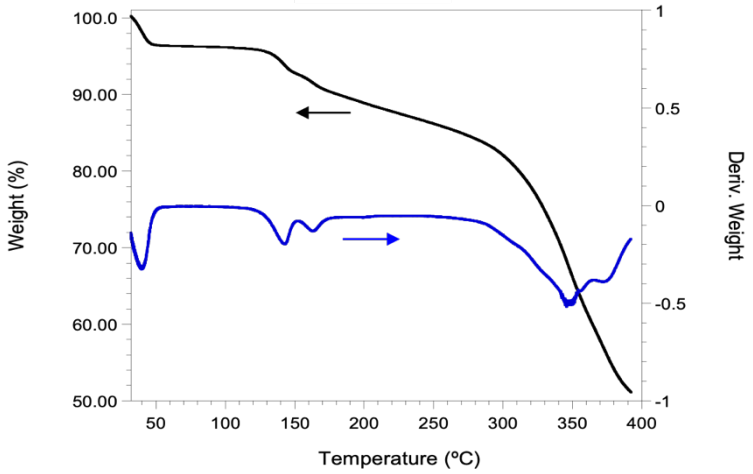

Figure S20. TG (left scale) and derivative (right scale) of compound **2**.

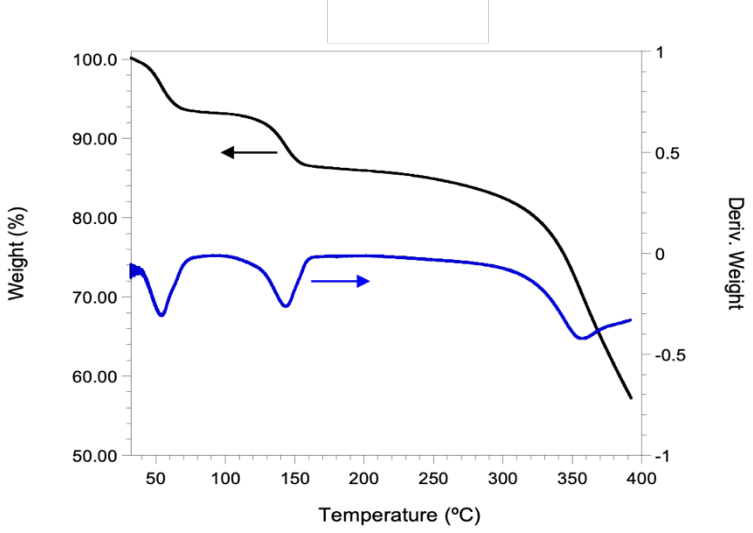

Figure S21. TG (left scale) and derivative (right scale) of compound **1/dmf/H_2O**.

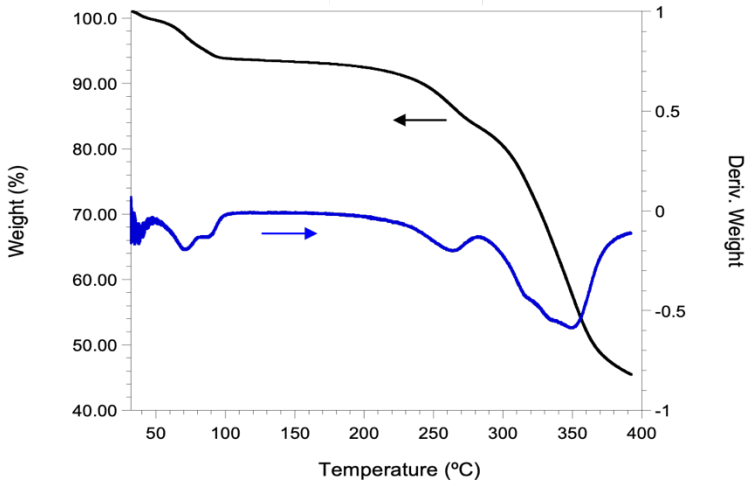

Figure S22. TG (left scale) and derivative (right scale) of compound **2/dmso**.

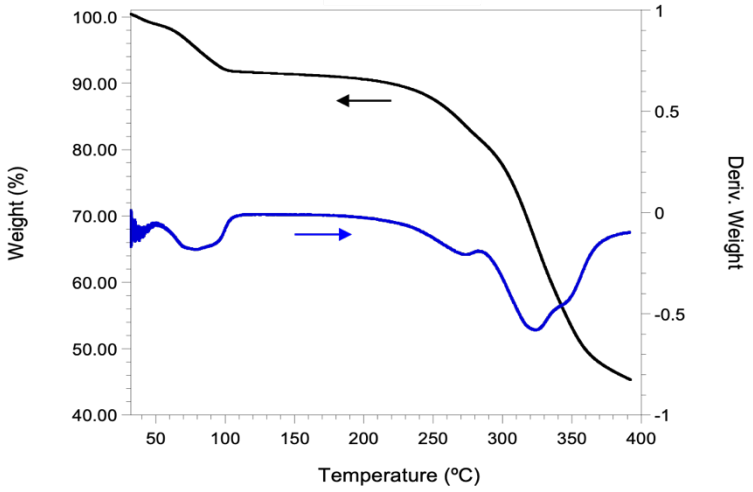

Figure S23. TG (left scale) and derivative (right scale) of compound **3**.

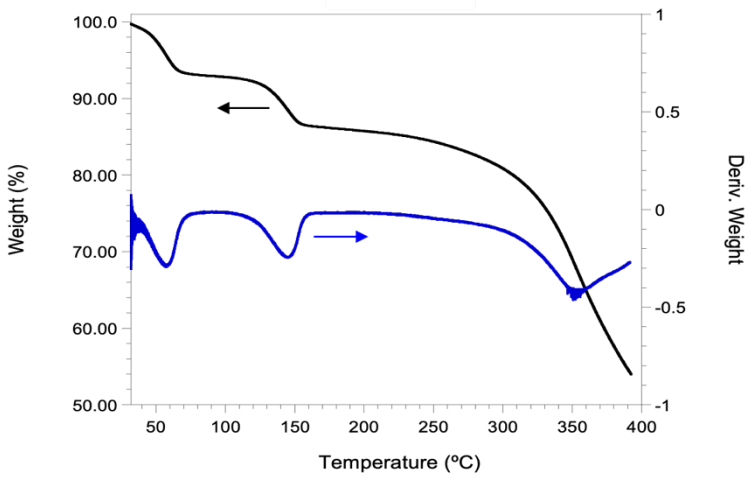

Figure S24. TG (left scale) and derivative (right scale) of compound **3/H_2O**.

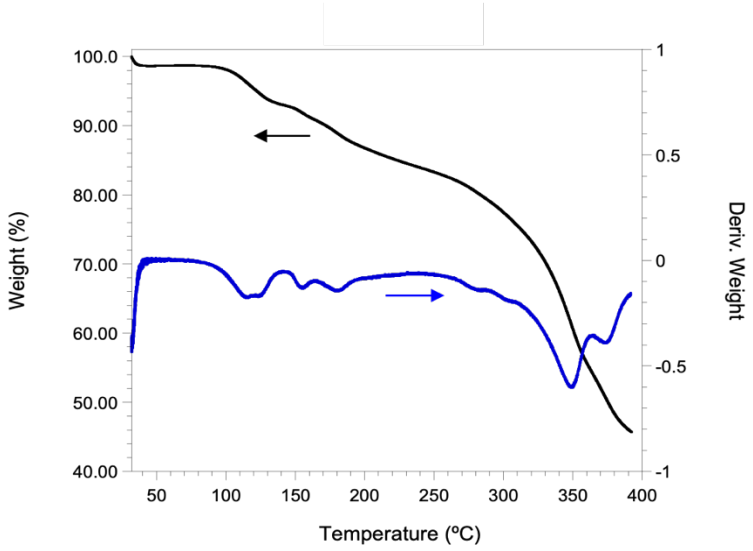

Figure S25. TG (left scale) and derivative (right scale) of compound **2/dmso/dmf**.

Table S8. Solvent content in the three water-containing samples (**1**, **1/dmf/H_2O** and **3/H_2O**) determined with TG measurements.

Sample	T (°C) 1st step	Weight loss 1st step (%)	H_2O Molecules	T (°C) 2nd step	Weight loss 2nd step (%)	H_2O Molecules
1	65-93	7.0	5.7	158-317	15.0	12.2
1/dmf/H_2O	76-122	6.8	5.6	160-306	14.6	11.9
3/H_2O	77-118	7.2	5.8	160-312	15.1	12.3

Table S9. Solvent content in the three dmf-containing samples (**2**, **1/dmf** and **2/dmso/dmf**) determined with TG measurements.

Sample	T (°C) 1st step	Weight loss 1st step (%)	dmf molecules	T (°C) 2nd step	Weight loss 2nd step (%)	dmf molecules
2	53-118	3.8	0.8	176-278	12.6	2.8
1/dmf	147-169	4.0/8.0	0.9/1.8	239-268	19.2	4.3
2/dmso/dmf	40-91	1.3	0.3	199-263	15.5	3.5

Table S10. Solvent content in the three dmso-containing samples (**3**, **3/H_2O/dmso** and **2/dmso**) determined with TG measurements.

Sample	T (°C) 1st step	Weight loss 1st step (%)	dmso molecules	H_2O molecules
3	106-197	8.7	1.4	2
3/H_2O/dmso	90-114	7.5	1.2	2
2/dmso	102-199	7.8	1.0	2

ELEMENTAL ANALYSIS

C, H, N and S analyses were performed with a Thermo Electron CHNS Flash 2000 analyser and with a Carlo Erba mod. EA1108 CHNS analyser. The results observed for the dmf-containing samples (**2**, **1/dmf** and **2/dmso/dmf**) indicate that two or three of the dmf molecules are lost when the samples are air dried, in agreement with the TGA data.

Tables S11-S13 show the results of the elemental analysis of all the compounds and the estimated number of solvent molecules from these analyses. Again, the results agree with those observed in the TGA and single crystal X-ray data except for the dmf-containing samples that show lower values due to the solvent loss when the samples are air dried. These results also confirm that the solvent exchange is complete in the dmf-containing samples and almost complete in the dmso-containing samples (where a residual amount of *ca*. 0.1 dmso molecules remain in the exchanged samples).

Table S11. Elemental analyses results (%) and solvent content in the three H_2O-containing samples (**1**, **1/dmf/H_2O** and **3/H_2O**) determined with elemental analysis measurements.

	Found (%)					Calc. (%)	
Sample	**C**	**H**	**N**	**S**	**n H_2O**	**C**	**H**
1	15.21	1.47	-	-	10	15.52	1.45
1/dmf/H_2O	15.15	1.55	0.01[a]	-	11	15.32	1.57
3/H_2O	15.31	1.40	-	0.18[b]	12	15.13	1.69

[a]This residual content is within experimental error and indicates that all the dmf molecules have been exchanged. [b]This residual content corresponds to *ca*. 0.1 dmso molecules remaining from the original compound **3**.

Table S12. Elemental analyses results (%) and solvent content in the three dmf-containing samples (**2**, **1/dmf** and **2/dmso/dmf**) determined with elemental analysis measurements.

	Found (%)					Calc. (%)		
Sample	**C**	**H**	**N**	**S**	**n dmf**	**C**	**H**	**N**
2	21.34	1.68	3.02	-	3	22.65	1.48	2.93
1/dmf	23.99	2.22	4.63	-	4	23.94	1.88	3.72
2/dmso/dmf	23.09	2.02	3.76	0.21[a]	5	25.12	2.23	4.44

[a]This residual content corresponds to *ca*. 0.1 dmso molecules remaining from the original compound **3**.

Table S13. Elemental analyses results (%) and solvent content in the three dmso-containing samples (**3**, **3/H_2O/dmso** and **2/dmso**) determined with elemental analysis measurements.

	Found (%)						Calc. (%)		
Sample	**C**	**H**	**N**	**S**	**n dmso**	**n H_2O**	**C**	**H**	**S**
3	20.81	2.02	-	10.29	2	2	20.98	2.35	11.20
3/H_2O/dmso	20.92	2.05	-	10.61	1	2	20.51	2.09	9.78
2/dmso	20.97	2.16	0.01[a]	10.71	2	1	21.20	2.25	11.32
					1	1	20.74	1.99	9.89
					2	0	21.43	2.16	11.44

[a]This residual content is within experimental error and indicates that all the dmf molecules have been exchanged.

OPTICAL PROPERTIES

Absorbance measurements were carried out in suspension. UV-visible spectra were measured with a HP 8453 spectrophotometer. Luminescence measurements were acquired both in solvent suspension and in solid state under the same excitation of 340 nm, i.e. coinciding with the maximum of the absorption band. To generate the excitation light, a BBO crystal was used to double the emission of a Ti:Sapphire laser operating at 680 nm. Then, the second harmonic emission was filtered, collimated and guided to an optical microscope. The microscope was adapted to achieve spectroscopy measurements in backscattering configuration. At the microscope, the sample was characterized using a 25 mm focal made of quartz as an objective, and hence, to focus the ultraviolet excitation light in a spot of around 200 μm diameter. After the microscope turret, the luminescence was filtered from excitation and dispersed in a 0.5 m monocromator and the resulting spectra were acquired by means of a silicon Peltier cooled photodiode array.

The slight increase in the intensity of P1 for compound **2** in dmf suspension suggests that the crystals of this compound can absorb some dmf molecules in the interlayer space and that these dmf molecule may interact via H-bonds with the O or Br atoms of the bromanilato ligand. This idea is supported by the fact that in compound **1** there are two H-bond (with $O_{water}\cdots O_{anilato}$ distances of 2.919 and 3.012 Å) and in compound **3** there is a S···O interaction (with a $S_{dmso}\cdots O_{anilato}$ distance of 3.302 Å) implying non coordinated solvent molecules and the O atoms of the anilato ligands (that

are connected to the Dy(III) ions). This fact indicates that the non coordinated solvents might also play a role in the luminescence of compounds **1**-**3**.

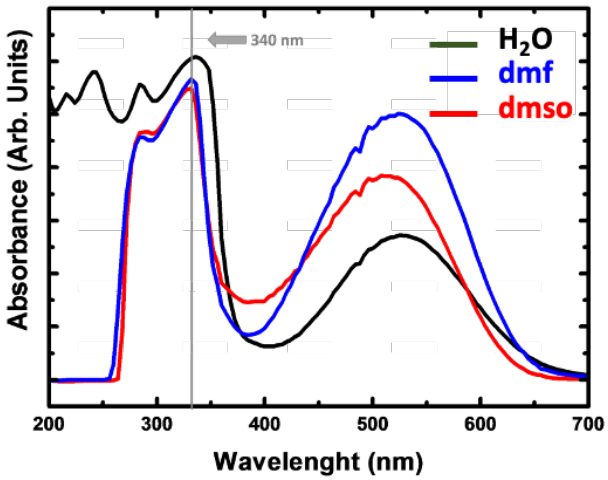

Figure S26. UV-vis absorbance spectra of bromanilic acid in H_2O, dmf and dmso.

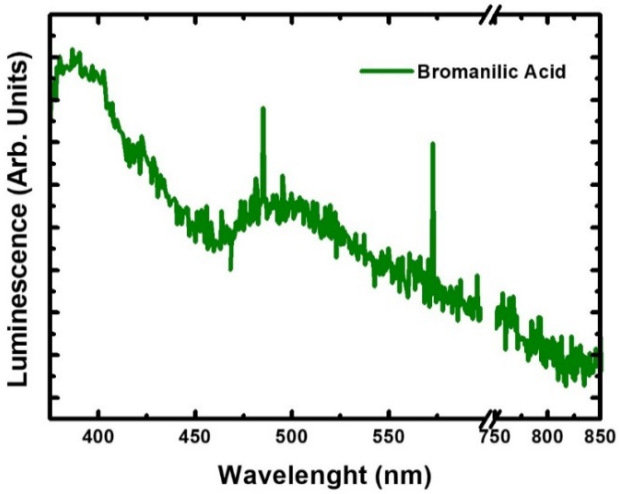

Figure S27. Luminescence emission spectrum of the free bromanilic acid in solid state (λ_{ex} = 340 nm).

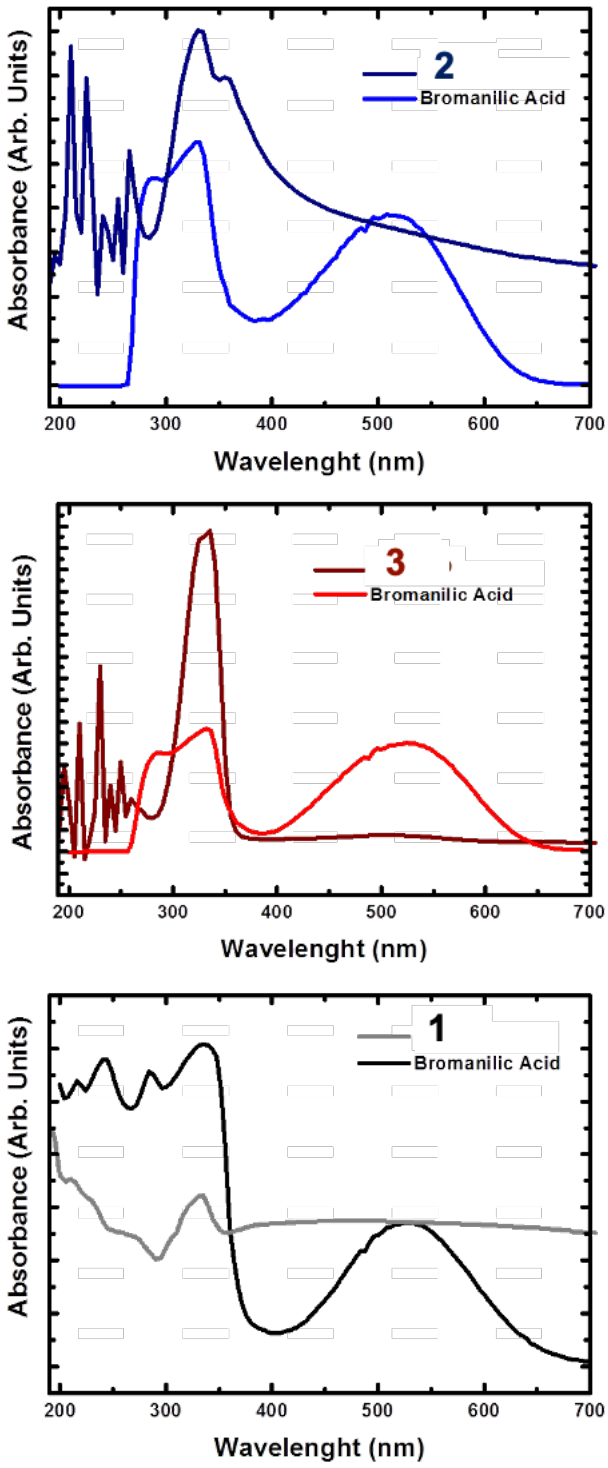

Figure S28. Comparison of the UV-vis absorbance spectra of **1**-**3** in solid state with bromanilic acid in the corresponding solvent.

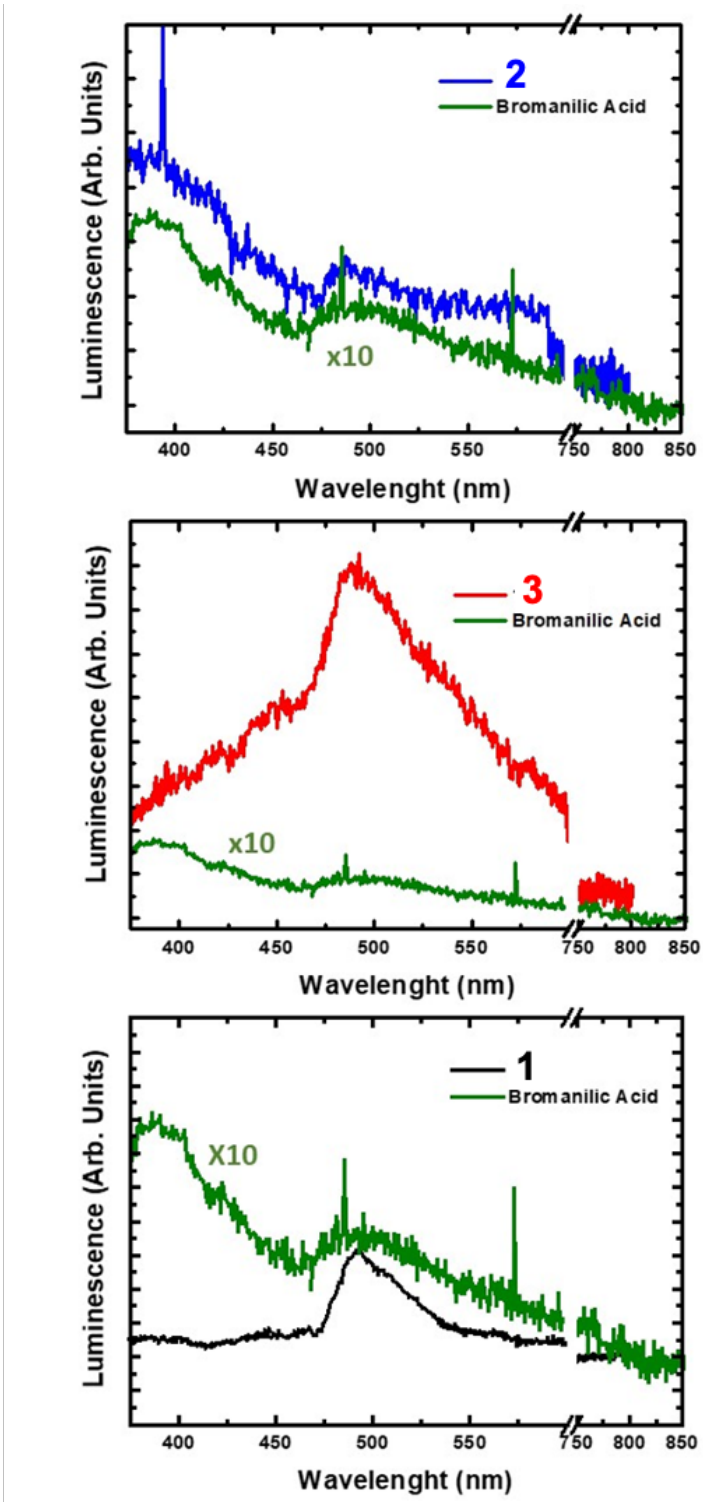

Figure S29. Comparison of the solid-state emission spectra of **1-3** with free bromanilic acid with λ_{ex} = 340 nm. (The intensity of the free bromanilic acid has been multiplied by 10 for a better comparison).

MAGNETIC PROPERTIES

Magnetic measurements were performed with a Quantum Design MPMS-XL-5 SQUID magnetometer with an applied magnetic field of 0.1 T in the 2-300 K temperature range on polycrystalline samples with masses of 21.762, 26.507 and 26.226 mg for compounds **1-3**, respectively. AC susceptibility measurements were performed on the same samples with an oscillating magnetic field of 4 Oe at low temperatures in the frequency range 10-10000 Hz with a Quantum Desing PPMS-9 and with different applied DC fields. Susceptibility data were corrected for the sample holder and for the diamagnetic contribution of the salts using Pascal's constants.[8]

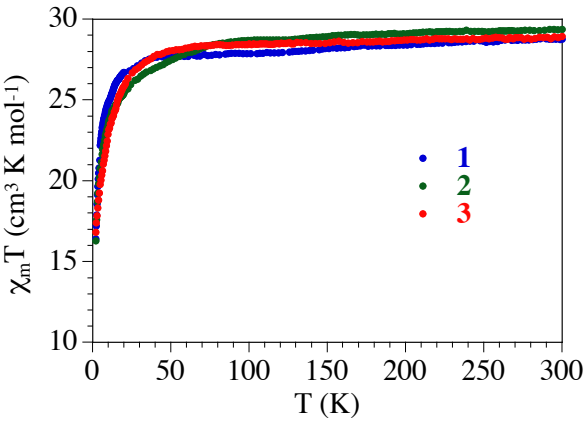

Figure S30. Thermal variation of the $\chi_m T$ product per formula unit for compounds **1-3**.

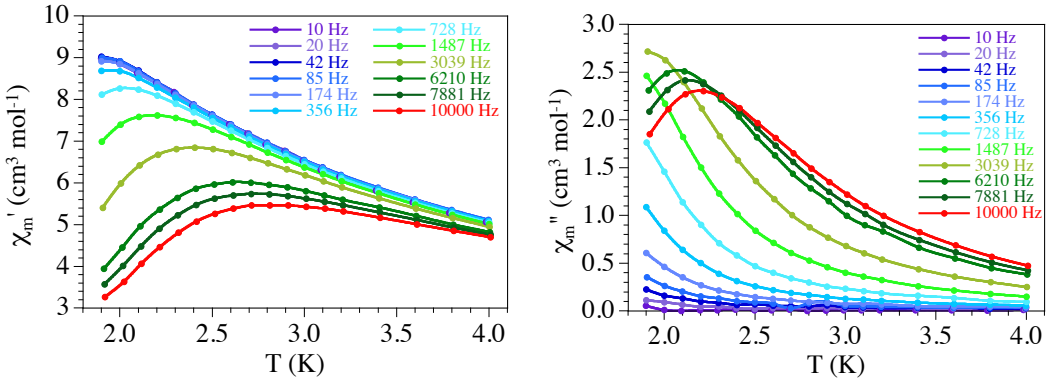

Figure S31. Thermal dependence of the in phase (**left**) and out-of-phase (**right**) AC signals at different frequencies in compound **1** with a DC field of 1000 Oe.

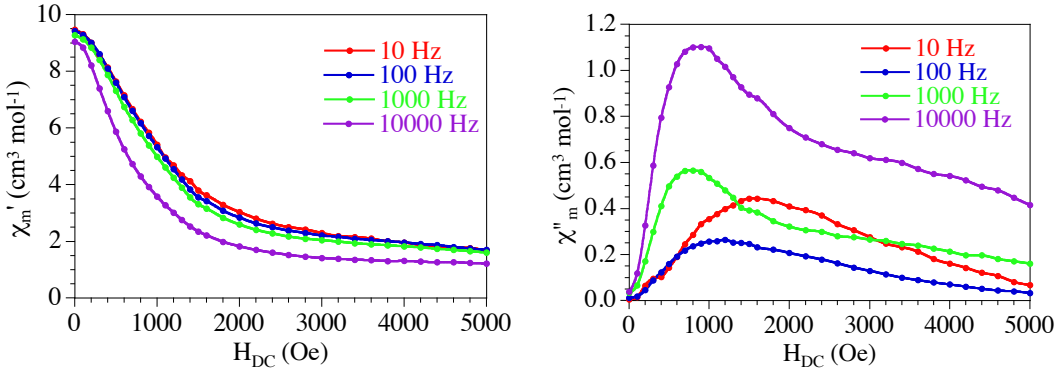

Figure S32. Field dependence of the in phase (**left**) and out-of-phase (**right**) AC signals at different frequencies at 2.0 K in compound **1**.

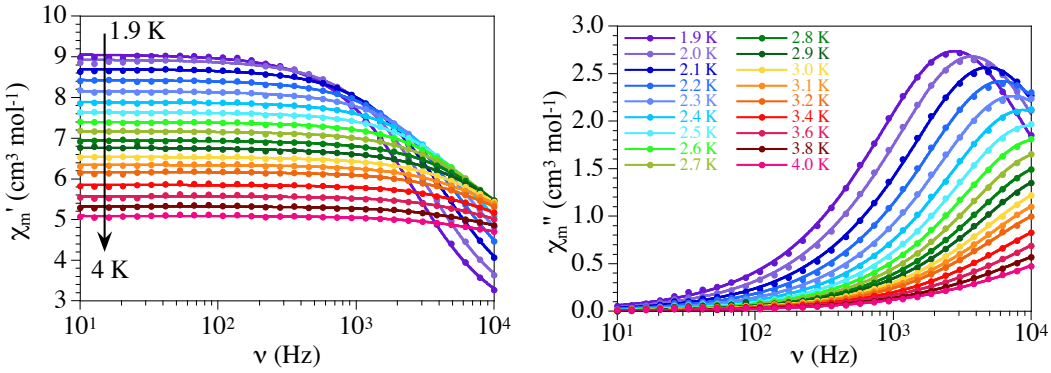

Figure S33. Frequency dependence of in phase (**left**) and out of phase (**right**) AC signals at different temperatures in compound **1** with a DC field of 1000 Oe. Solid lines are the best fit to the Debye model.

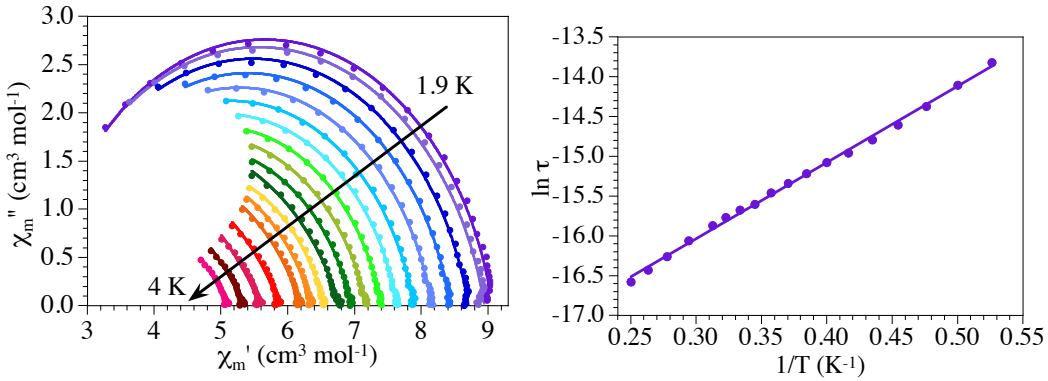

Figure S34. (**left**) Cole-Cole or Argand plot for compound **1** at different temperatures with a DC field of 1000 Oe. (**right**) Arrhenius plot of τ with the fit to equation 1 with only the Orbach term.

Table S14. Values of the parameters obtained by fitting the χ''_m values to the Debye model for compound **1** with a DC field of 1000 Oe.

T (K)	α	χ_S[a]	χ_T[a]	τ (s)
1.9	0.16552	3.4420	10.558	9.9314e-07
2.0	0.16246	3.5323	10.468	7.4786e-07
2.1	0.15946	3.6957	10.304	5.7151e-07
2.2	0.15752	3.8922	10.108	4.5425e-07
2.3	0.15211	4.1178	9.8822	3.7681e-07
2.4	0.14826	4.3232	9.6768	3.1845e-07
2.5	0.14337	4.5497	9.4503	2.8317e-07
2.6	0.14900	4.7079	9.2921	2.4652e-07
2.7	0.15432	4.8614	9.1386	2.1731e-07
2.8	0.16282	4.9961	9.0039	1.9372e-07
2.9	0.17904	5.0747	8.9252	1.6718e-07
3.0	0.18181	5.2280	8.7720	1.5571e-07
3.1	0.19148	5.3293	8.6707	1.4209e-07
3.2	0.19176	5.4771	8.5231	1.2816e-07
3.4	0.21980	5.5593	8.4406	1.0581e-07
3.6	0.27179	5.4220	8.5780	8.6814e-08
3.8	0.25903	5.8026	8.1974	7.3205e-08
4.0	0.29301	5.8029	8.1971	6.3166e-08

[a] in $cm^3\ mol^{-1}$ units

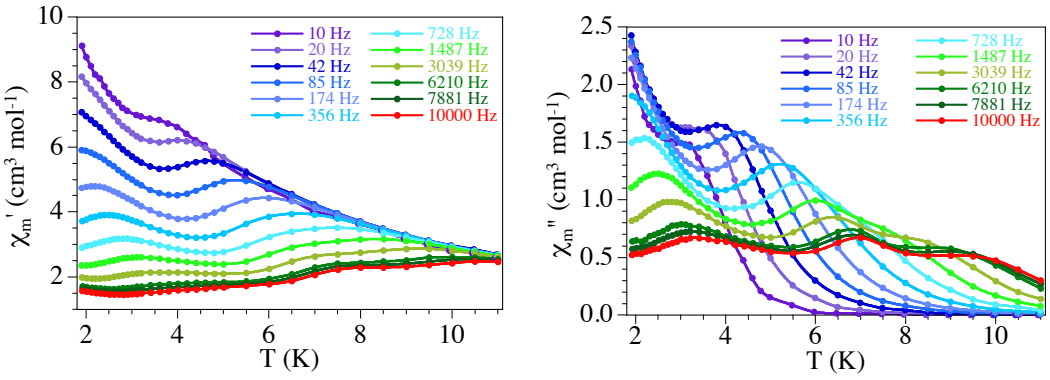

Figure S35. Thermal dependence of the in phase (**left**) and out-of-phase (**right**) AC signals at different frequencies in compound **2** with a DC field of 1000 Oe.

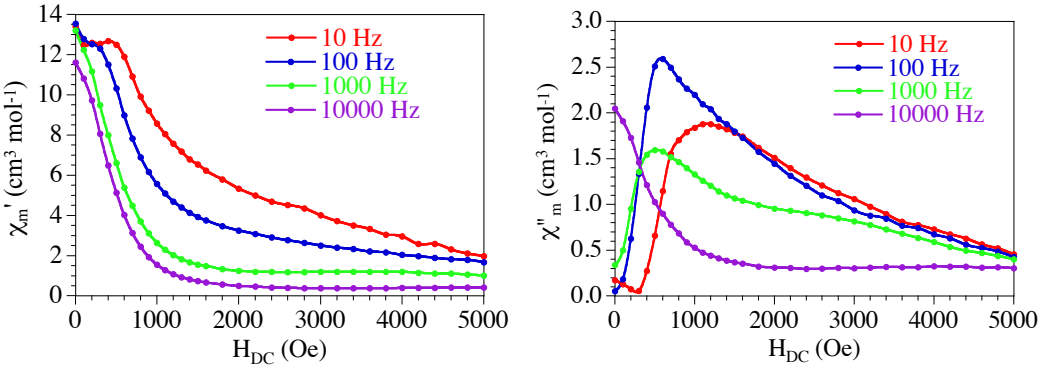

Figure S36. Field dependence of the in phase (**left**) and out-of-phase (**right**) AC signals at different frequencies at 2.0 K in compound **2**.

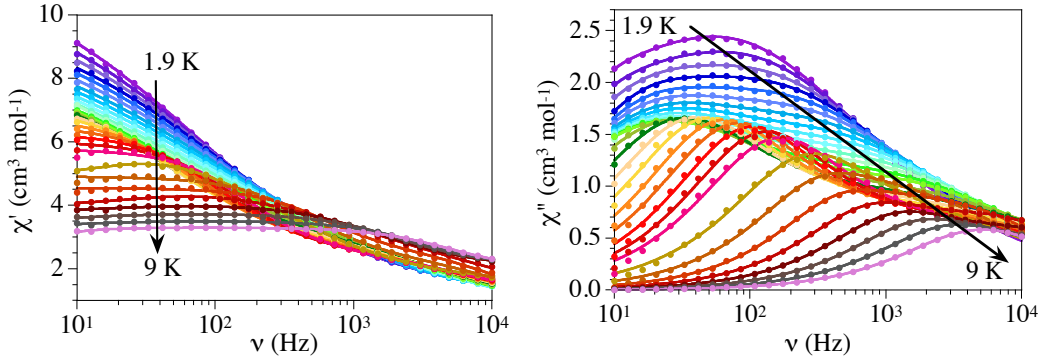

Figure S37. Frequency dependence of the in phase (**left**) and out of phase (**right**) AC signals at different temperatures in compound **2**. Solid lines are the best fit to the Debye model. with a DC field of 1000 Oe

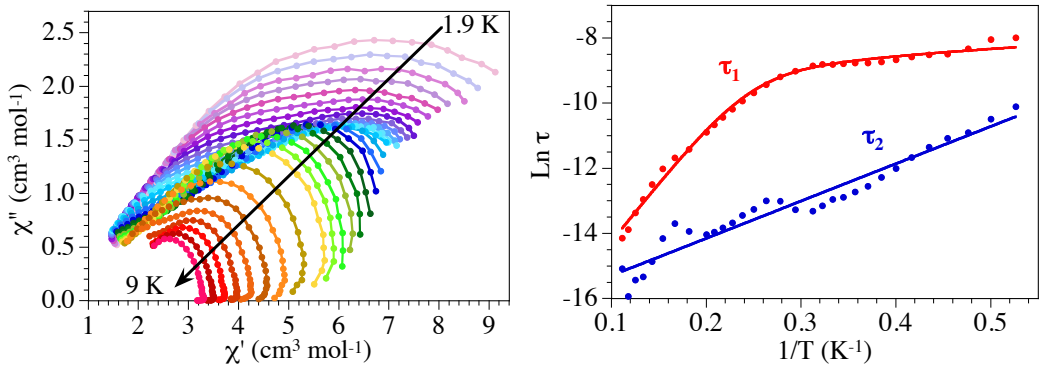

Figure S38. (**left**) Cole-Cole or Argand plot for compound **2** at different temperatures with a DC field of 1000 Oe. (**right**) Arrhenius plot of τ_1 (SR) and τ_2 (FR) with the fit to equation 1 with only the Orbach term (for τ_2) and Orbach plus Direct terms (for τ_1).

Table S15. Values of the parameters obtained by fitting the χ''_m values to two Debye models for compound **2** with a DC field of 1000 Oe.

T (K)	α_1	α_2	χ_S[a]	χ_{T1}[a]	χ_{T2}[a]	τ_1 (s)	τ_2 (s)
1.9	0.086605	0.45534	1.9917	2.7065	13.055	0.00033952	4.0666e-05
2.0	0.10113	0.44498	2.1442	3.6384	12.670	0.00031921	2.7959e-05
2.1	0.17559	0.43143	1.8373	4.1731	11.835	0.00024224	1.8467e-05
2.2	0.12490	0.43024	1.3587	3.5100	10.858	0.00020478	1.5523e-05
2.3	0.18169	0.42836	1.2869	3.9372	10.604	0.00019964	1.1855e-05
2.4	0.23692	0.41984	1.2164	4.5331	10.389	0.00018770	8.5756e-06
2.5	0.29175	0.40796	1.1071	5.1264	10.171	0.00017233	6.1145e-06
2.6	0.31351	0.40421	1.0432	5.4187	9.9861	0.00016171	4.6843e-06
2.7	0.35378	0.39578	0.89884	5.8391	9.8419	0.00015548	3.5247e-06
2.8	0.35690	0.39977	0.86687	5.8742	9.7132	0.00015559	2.9931e-06
2.9	0.35995	0.40159	0.85442	5.9496	9.5933	0.00015286	2.5268e-06
3.0	0.33327	0.42351	0.97436	5.7369	9.5073	0.00014919	2.3676e-06
3.1	0.35172	0.41744	0.86391	5.9546	9.4076	0.00014893	1.9407e-06
3.2	0.35623	0.42060	0.84914	6.0433	9.3165	0.00014247	1.6452e-06
3.4	0.26644	0.48228	1.2611	5.4808	9.2522	0.00012199	1.7231e-06
3.6	0.17231	0.55513	1.5306	4.8005	9.2869	0.00010189	2.2599e-06
3.8	0.12149	0.56919	1.7132	4.6722	9.1160	8.0068e-05	2.2765e-06
4.0	0.10490	0.54868	1.8525	4.8569	8.7723	6.2394e-05	1.7449e-06
4.2	0.089191	0.51205	1.8292	4.8350	8.2114	4.8506e-05	1.4545e-06
4.4	0.090461	0.48395	1.9781	5.0316	7.9644	3.7733e-05	1.1477e-06
4.6	0.081542	0.44273	2.0204	5.0407	7.5775	2.9531e-05	9.8807e-07
4.8	0.085679	0.41160	2.0173	5.0064	7.2310	2.3303e-05	8.7035e-07
5.0	0.091073	0.38648	2.0372	4.9501	6.9454	1.8561e-05	8.0762e-07
5.5	0.091578	0.32462	2.2821	4.7774	6.4810	1.1070e-05	8.9198e-07
6.0	0.041546	0.25807	2.5993	4.2233	6.2145	8.4464e-06	1.1346e-06
6.5	0.023013	0.22345	2.7839	4.1021	5.9916	6.0327e-06	7.1756e-07
7.0	0.046675	0.18695	2.8529	4.2091	5.7175	3.7542e-06	3.5293e-07
7.5	0.056946	0.14742	2.9008	4.2332	5.3424	2.3743e-06	2.2035e-07
8.0	0.060605	0.12009	2.4093	3.6368	4.4162	1.5701e-06	1.9940e-07
8.5	0.081585	0.012235	2.3790	3.6659	4.1211	9.3556e-07	1.2036e-07
9.0	0.072667	0.037000	2.4672	3.3936	3.8469	7.1798e-07	2.8165e-07

[a] in $cm^3\ mol^{-1}$ units

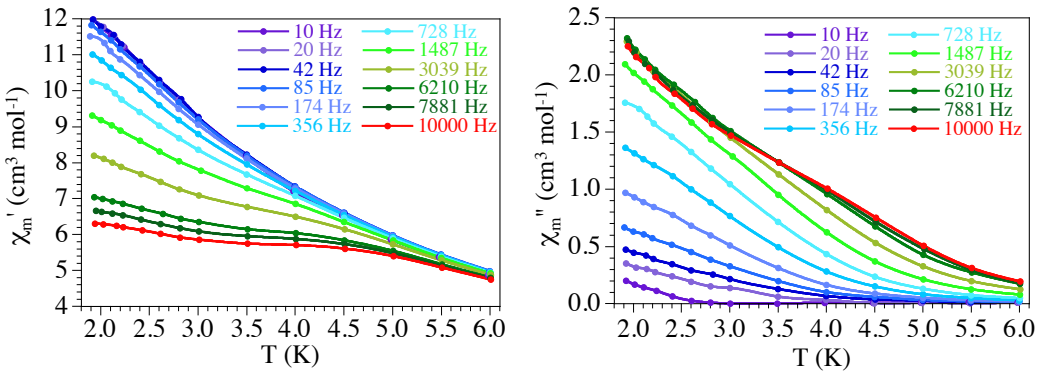

Figure S39. Thermal dependence of the in phase (left) and out-of-phase (right) AC signals at different frequencies in compound **3** with a DC field of 1000 Oe.

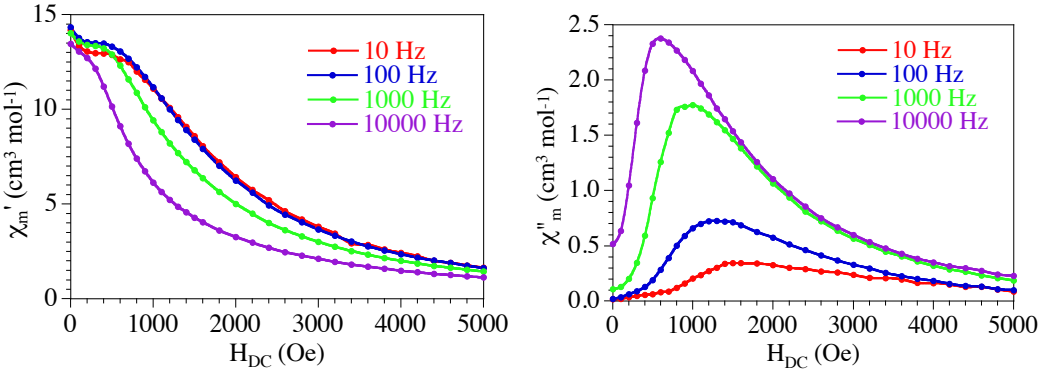

Figure S40. Field dependence of the in phase (left) and out-of-phase (right) AC signals at different frequencies at 2.0 K in compound **3**.

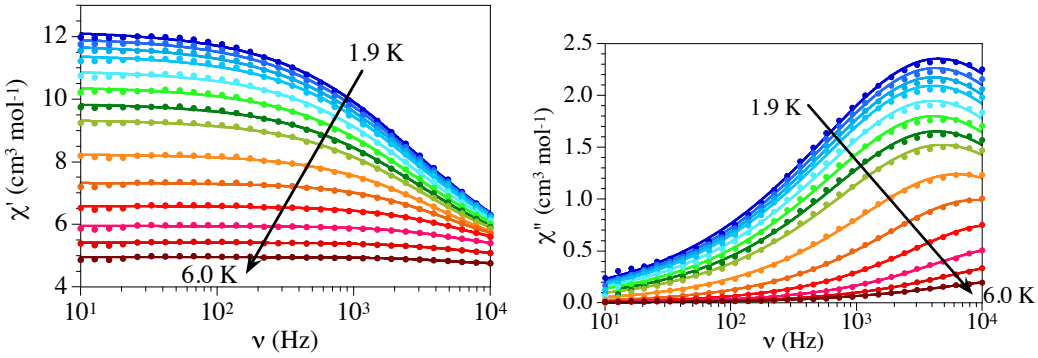

Figure S41. Frequency dependence of the in phase (left) and out of phase (right) AC signals at different temperatures in compound **3** with a DC field of 1000 Oe. Solid lines are the best fit to the Debye model.

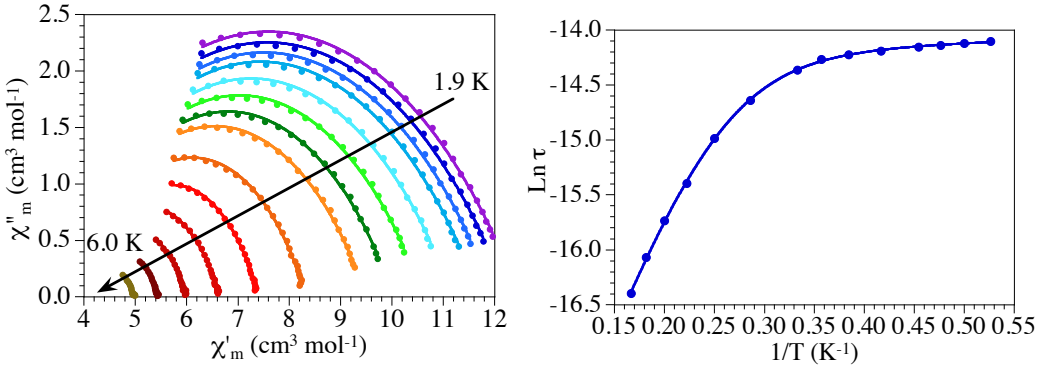

Figure S42. (left) Cole-Cole or Argand plot for compound **3** at different temperatures with a DC field of 1000 Oe. (right) Arrhenius plot of τ with the fit to equation 1 with the Orbach, Direct and Quantum tunneling terms.

Table S16. Values of the parameters obtained by fitting the χ''_m values to the Debye model for compound **3** with a DC field of 1000 Oe.

T (K)	α	χ_S[a]	χ_T[a]	τ (s)
1.9	0.43210	2.0781	11.922	7.2994e-07
2.0	0.42007	2.3805	11.619	7.2870e-07
2.1	0.41682	2.5921	11.408	7.2290e-07
2.2	0.40838	2.8246	11.175	7.1363e-07
2.4	0.39835	3.1924	10.808	6.8662e-07
2.6	0.39187	3.5272	10.473	6.6401e-07
2.8	0.38127	3.8707	10.129	6.3775e-07
3.0	0.37448	4.1538	9.8462	5.7881e-07
3.5	0.34654	4.8016	9.1984	4.3933e-07
4.0	0.30656	5.3635	8.6365	3.1035e-07
4.5	0.28735	5.7898	8.2102	2.0632e-07
5.0	0.28189	6.1413	7.8587	1.4648e-07
5.5	0.28433	6.4964	7.5036	1.0525e-07
6.0	0.33336	6.5940	7.4060	7.5661e-08

[a] in $cm^3\ mol^{-1}$ units

THEORETICAL CALCULATIONS

Table S17. Ab initio calculated low-lying spin-free energy states for compounds **1**-**3**.

1	2	3
0.000	0.000	0.000
15.989	14.996	12.928
201.136	271.743	203.213
220.305	312.310	227.219
247.779	349.611	319.578
307.644	426.267	367.885
369.155	497.345	422.277
470.433	541.941	500.985
504.417	569.505	524.387
514.727	734.262	751.071
537.863	752.228	755.327
7650.608	7750.673	7668.422
7699.026	7792.275	7693.817
7731.810	7811.941	7796.230
7755.160	7854.517	7858.388
7794.884	7922.570	7877.372

Table S18. Ab initio calculated low-lying spin-orbit energy states for compounds **1**-**3**.

1	2	3
0.000	0.000	0.000
0.000	0.000	0.000
120.226	193.454	141.905
120.226	193.454	141.905
171.659	281.367	230.742
171.659	281.367	230.742
199.273	357.934	308.088
199.273	357.934	308.088
239.265	436.165	361.902
239.265	436.165	361.902
309.106	489.821	411.251
309.106	489.821	411.251
398.061	545.575	499.494
398.061	545.575	499.494
421.898	688.436	704.174
421.898	688.436	704.174

Table S19: Single aniso computed energy of the KDs, g and wave functions composition for compound **1**.

Kramers doublets	Energy (cm^{-1})	g_x	g_y	g_z	Angle (°)	Wavefunction composition
1	0.000	0.114	0.198	19.123		86.54 % |±15/2> + 9.76 % |±11/2> + 2.19 % |±9/2>
2	120.226	1.431	3.245	13.804	20.98	56.85% |±13/2> + 14.51 % |±9/2> + 10.48 % |±7/2> + 5.48 % |±3/2> + 4.5 % |±11/2> + 3.77 % |±1/2> + 3.71 % |±5/2>
3	171.659	1.040	1.372	13.383	88.52	26.32 % |±5/2> + 15.20 % |±13/2> + 12.68 % |±7/2> + 13.26 % |±3/2> + 14.74% |±1/2> + 10.74 % |±9/2> + 5.10 % |±11/2>
4	199.273	8.905	6.432	3.112	74.01	39.42 % |±11/2> + 16.57 % |±7/2> + 14.38 % |±9/2> + 13.04 % |±3/2> + 6.41 % |±1/2> + 4.87 % |±5/2> + 2.67 % |±15/2>
5	239.265	1.065	3.741	12.726	92.25	27.45 % |±9/2> + 20.23 % |±7/2> + 17.61 % |±1/2> + 12.72 % |±5/2> + 10.95 % |±3/2> + 7.23 % |±11/2> + 2.6 % |±13/2>
6	309.106	1.111	1.208	14.062	88.80	24.94 % |±5/2> + 21.42 % |±7/2> + 16.72 % |±3/2> + 8.56 % |±1/2> + 8.85 % |±9/2> + 10.05 % |±11/2> + 6.95 % |±13/2>
7	398.061	0.309	0.360	19.453	56.59	20.97 % |±11/2> + 18.55 % |±9/2> + 13.25 % |±7/2> + 13.73 % |±13/2> + 12.23 % |±5/2> + 9.98 % |±3/2> + 6.99 % |±1/2> + 4.27 % |±1/2>
8	421.898	0.158	0.494	18.454	90.84	41.67 % |±1/2> + 30.36 % |±3/2> + 14.78 % |±5/2> + 5.05 % |±7/2> + 3.09 % |±9/2> + 3.63 % |±11/2> + 1.53 % |±11/2>

Table S20: Single aniso computed energy of the KDs, g and wavefuctions composition for compound **2**.

Kramers doublets	Energy (cm^{-1})	g_x	g_y	g_z	Angle (°)	Wavefunction composition
1	0.000	0.004	0.005	19.832		97.98 % |±15/2> + 1.19 %| ± 7/2>
2	193.454	0.155	0.204	16.922	10.17	88.84 % |±13/2> + 5.5 % |±11/2> + 2 % |±9/2> + 3.22 % |±7/2>
3	281.367	0.537	0.855	14.299	19.59	66.93 % |±11/2> + 23.38 % |±9/2> + 4.47 % |±5/2> + 2.63 % |±13/2> + 1.81 % |±7/2>
4	357.934	1.891	3.097	10.986	19.95	40.09 % |±9/2> + 35.74 % |±7/2> + 9.78 % |±11/2> + 6.42 % |±3/2> + 4.45%| ± 13/2> + 0.69%|±15/2>
5	436.165	7.755	5.822	1.081	90.33	25.73 % |±7/2> + 34.44 % |±5/2> + 14.96 % |±9/2> + 13.61 % |±11/2> + 8.13 % |±1/2> + 2.09 % |±13/2> + 0.57 % |±15/2>
6	489.821	2.634	4.824	13.112	79.33	31.38 % |±3/2> + 23.80 % |±5/2> + 17.92 % |±1/2> + 11.65% |±7/2> + 10.90 % |±9/2> + 2.57 % |±11/2> + 1.39 % |±13/2>
7	545.575	0.550	0.974	15.929	99.69	25.22 % |±1/2> + 31.04 % |±3/2> + 20.22 % |±5/2> + 16.29 % |±7/2> + 6.22 % |±9/2> + 0.52 %| ± 11/2>
8	688.436	0.049	0.129	19.517	88.41	47.37 % |±1/2> + 30.30 % |±3/2> + 15.09 % |±5/2> + 5.44 % |±7/2> + 1.16 % |±9/2>

Table S21: Single-aniso computed energy of the KDs, g and wavefuctions composition for compound **3**.

Kramers doublets	Energy (cm^{-1})	g_x	g_y	g_z	Angle (°)	Wavefunction composition
1	0.000	0.017	0.031	19.57		93.21 % |±15/2> + 6.2 % |±11/2>
2	141.905	0.429	0.711	16.175	17.99	70.1 % |±13/2> + 18.52 % |±9/2> + 5.2 % |±11/2> + 1.25 % |±7/2> + 2.7 % |±5/2>
3	230.742	1.338	2.004	12.699	26.75	30.3 % |±11/2> + 25 % |±7/2> + 14 % |±13/2> + 10.18 % |±9/2> + 7.2 % |±5/2> + 7 % |±3/2> + 2.9 % |±1/2> + 2.8 % |±15/2>
4	308.088	9.142	5.809	1.872	104.38	25.3 % |±11/2> + 19.37 % |±5/2> + 18.1 % |±1/2> + 12 % |±7/2> + 11.83 % |±3/2> + 9.34 % |±9/2> + 2.5 % |±13/2>
5	361.902	2.717	4.522	10.577	90.96	27 % |±1/2> + 22 % |±3/2> + 19.5 % |±9/2> + 12 % |±5/2> + 8.5 % |±7/2> + 5.8 % |±11/2> + 4.8 % |±13/2>
6	411.251	0.911	1.611	16.6	76.70	29.52 % |±5/2> + 21 % |±7/2> + 22.4 % |±3/2> + 10.26 % |±9/2> + 8.96 % |±1/2> + 5.71 % |±11/2> + 1.78 % |±13/2>
7	499.494	0.034	0.051	18.546	90.92	39.24 % |±1/2> + 28 % |±3/2> + 12.51 % |±5/2> + 6.42 % |±7/2> + 6.7 % |±9/2> + 4.93 % |±11/2>
8	704.174	0.001	0.002	19.853	59.06	25.32 % |±9/2> + 25.33 % |±7/2> + 15.70 % |±11/2> + 16.66 % |±5/2> + 5.58 % |±13/2> + 6.4 % |±13/2> + 7.55 % |±3/2> + 2.9 % |±3/2>

Table S22: Single aniso computed crystal field parameters for compounds **1-3**.

k	Q	**1**	**2**	**3**
2	-2	-0.7840E+00	-0.1138E+01	-0.1946+01
	-1	-0.1568E+01	-0.2276E+01	-0.3892E+01
	0	-0.1356E+01	-0.3178E+01	-0.2215E+01
	1	0.1670E+01	-0.2037E+01	0.3687E+01
	2	0.1939E+01	0.1264E+00	0.2457E+01
4	-4	-0.5791E-02	-0.1004E-01	-0.5150E-02
	-3	-0.1637E-01	-0.2841E-01	-0.1456E-01
	-2	-0.4377E-02	-0.7593E-02	-0.3893E-02
	-1	-0.6190E-02	-0.1073E-01	-0.5506E-02
	0	-0.2076E-02	-0.7135E-03	-0.4900E-02
	1	0.1270E-01	0.8660E-02	-0.5064E-02
	2	0.1037E-01	-0.6908E-02	0.2711E-01
	3	0.1924E-01	0.2655E-01	0.3677E-01
	4	-0.1584E-02	-0.2578E-02	-0.1038E-01
6	-6	0.3095E-03	-0.2830E-05	0.6407E-04
	-5	0.1072E-02	-0.9804E-05	0.2219E-03
	-4	0.2286E-03	-0.2090E-05	0.4732E-04
	-3	0.4174E-03	-0.3816E-05	0.8639E-04
	-2	0.2087E-03	-0.1908E-05	0.4319E-04
	-1	0.2640E-03	-0.2413E-05	0.5464E-04
	0	-0.1995E-04	-0.2347E-04	0.3448E-05
	1	-0.1215E-03	0.5136E-04	-0.1860E-03
	2	0.2156E-03	-0.3157E-04	-0.4891E-04
	3	0.3415E-03	0.4072E-03	0.1082E-03
	4	0.2161E-03	-0.6320E-04	0.6076E-04
	5	0.5943E-04	-0.2447E-03	0.5863E-03
	6	0.1193E-03	-0.2157E-03	0.1233E-03

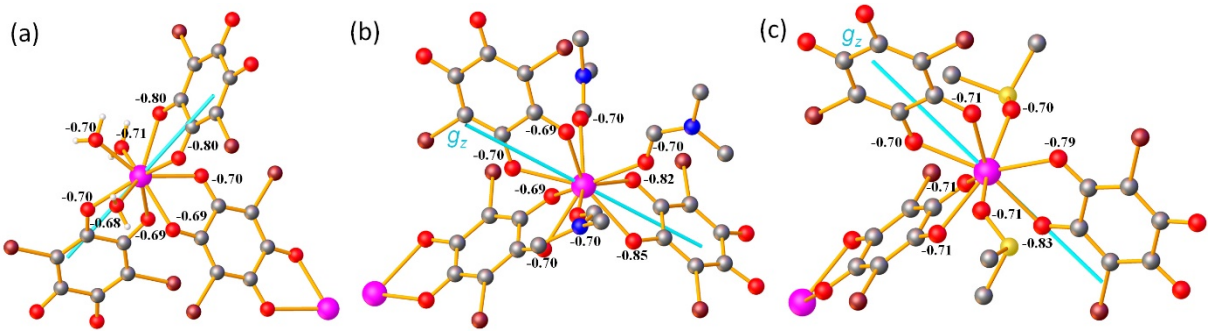

Figure S43. Orientation of the ground state anisotropy axis and LoProp charges of the coordinating atoms for compounds **1 (a)**, **2 (b)** and **3 (c)**.

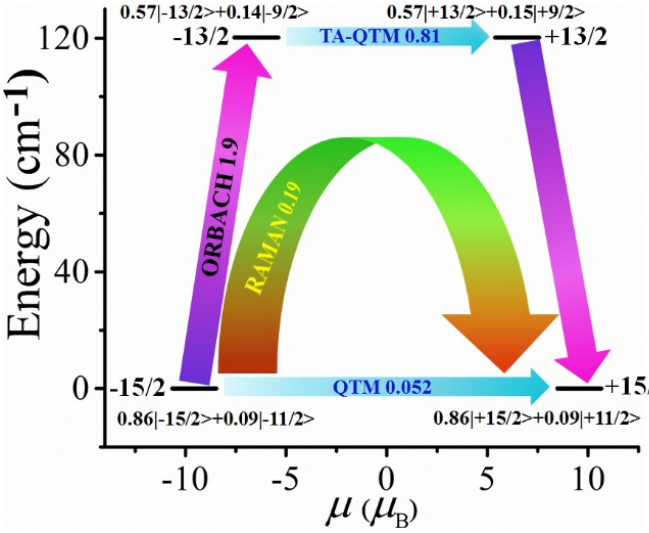

Figure S44. Ab initio calculated blocked barrier for compound **1**.

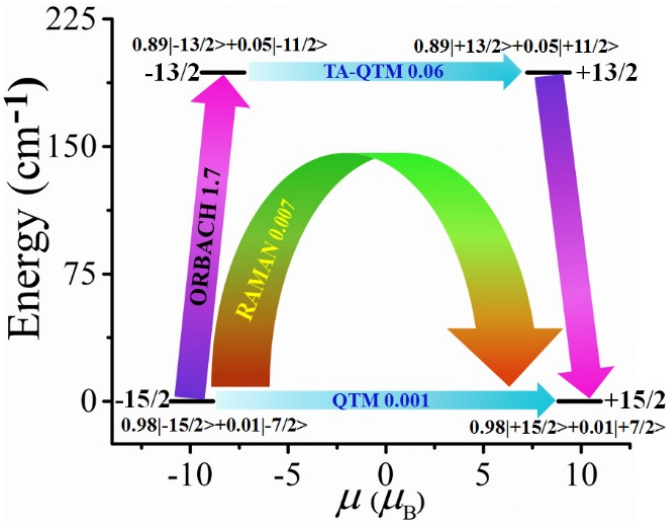

Figure S45. Ab initio calculated blocked barrier for compound **2**.

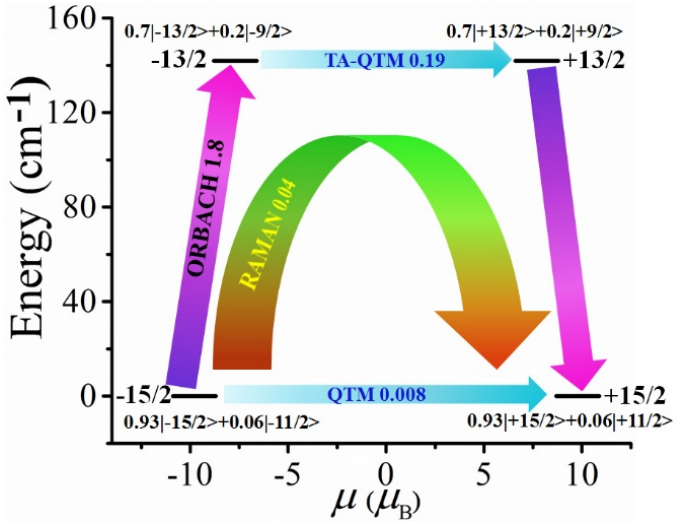

Figure S46. Ab initio calculated blocked barrier for compound **3**.

Computational Details

In order to investigate the electronic structure and magnetic properties, we have performed ab initio calculations for all the compounds. All the calculations were CASSCF/RASSI-SO/Single-Aniso type and carried out on the coordinates of the reasonable fragments obtained from X-ray crystal structure. In this regard, the Yb(III) ion was replaced by the Dy(III) ion for compound **1** as it is isostructural with the corresponding Dy(III) analog compound. In the studied compounds, the exchange coupling between two metal centers is very weak and the blockage of the magnetization reversal process mainly arises from the individual metal centers. The ab initio calculations were performed on Dy(III) ions using MOLCAS 8.2 software package.[9] We have employed the relativistic basis sets from ANO-RCC library, ANO-RCC...9s8p6d4f3g2h for Dysprosium, ANO-RCC...7s6p4d2f1g for Bromine, ANO-RCC...3s2p1d for Sulphur, Nitrogen, Oxygen, ANO-RCC...3s2p for Carbon and ANO-RCC...2s for Hydrogen. The Douglas-Kroll Hamiltonian[10] has been used to consider the relativistic effects. The spin-free Eigen states were obtained by CASSCF method[11] which was performed with the active space of 9 electrons in 7 orbitals (CAS 9,7). These active spaces were also used for state average calculations over 21 sextets for Dy(III) ions. We have also employed the RASSI-SO[12] to introduce the spin-orbit coupling within the space of spin-free eigen states. The Single-Aniso module[13] has been used to compute the g tensor and crystal field parameters considering the previously calculated spin-orbit states. In addition, the Cholesky decomposition for 2-eletron integrals was used throughout the calculations to save disk space.

REFERENCES

1 G. López-Martínez, *PhD. Thesis. University of Valencia.,* 2017,

2 S. Benmansour, A. Hernández-Paredes, C. J. Gómez-García, *J. Coord. Chem.,* 2018, *71,* 845-863.

3 O. V. Dolomanov, L. J. Bourhis, R. J. Gildea, J. A. K. Howard, H. Puschmann, *J. Appl. Cryst.,* 2009, *42,* 339-341.

4 G. M. Sheldrick, *Acta Cryst. C,* 2015, *71,* 3-8.

5 M. Llunell, D. Casanova, J. Cirera, J. M. Bofill, P. Alemany, S. Alvarez, M. Pinsky, D. Avnir, 2013, *2.3,*

6 A. Ruiz-Martínez, D. Casanova, S. Alvarez, *Chem. Eur. J.,* 2008, *14,* 1291-1303.

7 D. Casanova, M. Llunell, P. Alemany, S. Alvarez, *Chem. Eur. J.,* 2005, *11,* 1479-1494.

8 G. A. Bain, J. F. Berry, *J. Chem. Educ.,* 2008, *85,* 532-536.

9 F. Aquilante, J. Autschbach, R. K. Carlson, L. F. Chibotaru, M. G. Delcey, L. De Vico, I. Fdez. Galván, N. Ferré, L. M. Frutos, L. Gagliardi, M. Garavelli, A. Giussani, C. E. Hoyer, G. Li Manni, H. Lischka, D. Ma, P. Å. Malmqvist, T. Müller, A. Nenov, M. Olivucci, T. B. Pedersen, D. Peng, F. Plasser, B. Pritchard, M. Reiher, I. Rivalta, I. Schapiro, J. Segarra-Martí, M. Stenrup, D. G. Truhlar, L. Ungur, A. Valentini, S. Vancoillie, V. Veryazov, V. P. Vysotskiy, O. Weingart, F. Zapata and R. Lindh, *J. Comput. Chem.*, 2016, 37, 506-541.

10 B. A. Heβ, C. M. Marian, U. Wahlgren and O. Gropen, *Chem. Phys. Lett.*, 1996, *251*, 365-371.
11 B. O. Roos and P.-Å. Malmqvist, *PCCP*, 2004, *6*, 2919-2927.
12 P. Å. Malmqvist, B. O. Roos and B. Schimmelpfennig, *Chem. Phys. Lett.*, 2002, *357*, 230-240.
13 L. F. Chibotaru and L. Ungur, *J. Chem. Phys.*, 2012, *137*, 064112.